Technical Report
RAL-TR-97-020

The NIMP (Non-LTE Ionised Material Package) Code

S J Rose

May 1997

COUNCIL FOR THE CENTRAL LABORATORY OF THE RESEARCH COUNCILS

Enquiries about copyright, reproduction and requests for additional copies of this report should be addressed to:

The Central Laboratory of the Research Councils
Library and Information Services
Rutherford Appleton Laboratory
Chilton
Didcot
Oxfordshire
OX11 0QX
Tel: 01235 445384 Fax: 01235 446403
E-mail library@rl.ac.uk

ISSN 1358-6254

The NIMP (Non-LTE Ionised Material Package) code

S.J.Rose
Rutherford Appleton Laboratory,
Chilton,
Didcot,
Oxon, OX11 0QX,
U.K.

1. Introduction

High-power laser-produced plasmas are, in general, far from Local Thermodynamic Equilibrium (LTE). The distribution of ions in the plasma, both between and within ionisation stages is not described by the equations of statistical equilibrium (usually written as the Saha/Boltzmann equations). In general, the populations are not in a steady-state (although this is a good approximation for some plasmas) and the distribution not only depends on the local conditions in the plasma, but also on its time-history. In this report we describe a simple model, which has its origins in the work of Grasberger (1965, 1966) and Lokke and Grasberger (1977) who describe an 'average-atom' method of calculating, in an approximate manner, the excitation/ionisation characteristics of a non-LTE plasma. The method usually employed to calculate the distribution of excitation/ionisation in a non-LTE system is to solve the rate-equations for all the important ionic states. The resulting coupled differential equations can be solved for each ionic state and, given a time-history of the electron temperature and density, the time evolution of the different ionic states in the plasma can be evaluated. However with lower temperatures and/or higher atomic number, the electronic structure of the ions involves open L-, M-... shells. For these cases, following the time-evolution of the number density of individual ionic states becomes very time-consuming and although limited calculations for open L-shell ions have been performed, the plethora of states which must be considered for open M-, N-... shell ions means that such detailed accounting is in practice impossible. Plasmas containing such ions occur frequently in laboratory and in particular, laser-produced plasmas. As a consequence, Grasberger (1965, 1966) and Lokke and Grasberger (1977) extended the 'average-atom' model originally proposed for LTE plasmas by Mayer (1947) to the non-LTE case. Although we shall look at the details of an 'average-atom' later, qualitatively, its utility arises because instead of following the time-evolution of individual ionic states, it follows the time-evolution of principal quantum shell occupancies, ('or shell populations') averaged over the distribution of ionic states. As a consequence, the shell occupancies are non-integral. By following the shell populations in time we reduce the number of differential equations in comparison with what is needed for a model which follows individual ionic states. This results in a great saving of computer time and also allows the possibility of tackling problems involving open L-, and particularly open M-, N- ..... shells. The non-LTE average-atom model may, therefore appear to be removing so much information in the averaging process that its use, particularly for spectroscopy, is severely limited. However, the shell populations can be used, at any time, to calculate the probability of an individual ionic state. In this way the level of detail of a calculation which follows individual ionic states can be reconstructed from the average-atom model. This may appear to be getting something for nothing, but the

approximation that has to be made in this procedure (and also in setting up the differential equations for the shell populations) is that there is no correlation between electrons occupying different shells. This is the fundamental approximation at the core of the non-LTE average-atom model described here and it gives the model its power and utility as well as being responsible for some of its shortcomings. We shall look at it in more detail in Section 3.1.

NIMP (Non-LTE Ionised Material Package) is the name given to the version of the non-LTE average atom model at the Rutherford Appleton Laboratory. It is based on the model described by Lokke and Grasberger (1977) with several features removed, changed or added to. In particular it allows a calculation of the distribution of ionic states from the average shell populations. It does not include many of the recent changes which have been made to the non-LTE average-atom code at LLNL and LANL, such as the inclusion of the effects of electron degeneracy and of pressure ionisation. The RAL version also uses a simple iterative scheme for the solution of the rate equations, which, whilst more time-consuming, does produce an accurate solution. Whilst not as sophisticated as the non-LTE average-atom codes at LLNL and LANL (Pollak 1990), NIMP has been used successfully in the design and analysis of many (particularly laser-plasma) experiments some of which are described later.

2. The NIMP (Non-LTE Ionised Material Package) code

NIMP can be run as a stand-alone package or interfaced to a hydrodynamics code. It is the former version which is described here. The package takes as input the nuclear charge Z, the atomic weight A and the time-histories of the electron temperature $T_e(t)$, the material density $\rho(t)$ and the radiation temperature $T_r(t)$. It also needs the number of shells to be considered (*nmax*) and the convergence accuracy (*xtest*). The populations of the principal quantum shell n at time t is denoted $P_n(t)$. It can be thought of as the number of electrons in shell n per ion, averaged over the different ions in the plasma, at time t. The initial populations $P_n(t=0)$ $(n=1 \rightarrow nmax)$ can also be provided by the user although default values are supplied. NIMP produces as output, at times requested by the user, the population of each shell $P_n(t)(n=1 \rightarrow nmax)$ and the probability of a particular ionic state, or group of states occurring in the plasma.

The average-atom model is different from a detailed model in that we construct differential equations for the time evolution of $P_n(t)$ by considering the average rate of populating and depopulating a particular shell. The processes which we are considering are collisional excitation and ionisation (by free electrons in the plasma) and their inverse processes: collisional deexcitation and three-body recombination. We also include the spontaneous and stimulated radiative rates, both between one bound level and another and between the continuum and a bound level. Figure 1(a) shows the collisional rates (denoted R^c) which populate and depopulate shell n. In figure 1(b) the spontaneous and stimulated radiative rates (denoted R^r) which populate and depopulate shell n are shown. We define the rate R to be the rate per electron in the initial shell, assuming that the final shell is empty. This allows us to use simple scaled hydrogenic rate formulae (described later) but introduces the complication that for a collisional excitation, for example, from level m to n (figure 1), the contribution to dP_n/dt has the form

$$P_m \left[1 - \frac{P_n}{2n^2} \right] R^c_{m \rightarrow n}$$

The first term P_m multiplies the one-electron rate by the number of electrons in the initial shell m. Because the rate R assumes that the final level is empty it is also multiplied by $1-(P_n/2n^2)$, usually referred to as Q_n, which is the fraction of the shell which is, on average, empty. This factor arises physically from the Pauli principle and plainly has the correct limiting form for an empty ($P_n=0$) and full ($P_n=2n^2$) shell n. We are however making here the fundamental approximation that there is no correlation between the occupancies of shell m and n (More, Zimmerman and Zinamon 1988). By adding together terms of this kind, we can construct the differential equations governing the time-evolution of the shell populations.

$$\frac{dP_n}{dt} =$$

$$\sum_{m=1}^{n-1} P_m Q_n R_{m\to n} + \sum_{r=n+1}^{nmax} P_r Q_n R_{r\to n} + Z^* Q_n R_{c\to n} \qquad (1)$$

$$-\sum_{m=1}^{n-1} P_n Q_m R_{n\to m} - \sum_{r=n+1}^{nmax} P_n Q_r R_{n\to r} - P_n R_{n\to c}$$

where the rate denoted R is the sum of the collisional and radiative terms

$$R = R^c + R^r. \qquad (2)$$

Z^* is the number of electrons per ion in the continuum c (free electrons)

$$Z^* = Z - \sum_{k=1}^{nmax} P_k \qquad (3)$$

and are treated as effectively occupying another shell which has population Z^*. Because the free electrons are treated as having a non-degenerate Maxwell-Boltzmann distribution the continuum has Q=1. The first line of the right hand side of equation (1) represents the terms which populate, whilst the second line represents terms which depopulate level n. The population terms have a common factor Q_n, whilst the depopulation terms have a common factor P_n, and the rate equations can be usefully written as

$$\frac{dP_n}{dt} = A_n Q_n - B_n P_n, \qquad (4)$$

where

$$A_n = \sum_{m=1}^{n-1} P_m R_{m\to n} + \sum_{r=n+1}^{nmax} P_r R_{r\to n} + Z^* R_{c\to n} \qquad (5)$$

$$B_n = \sum_{m=1}^{n-1} Q_m R_{n\to m} + \sum_{r=m+1}^{nmax} Q_r R_{n\to r} + R_{n\to c} \qquad (6)$$

There are *nmax* such coupled non-linear first-order differential equations which describe the time-evolution of the shell populations.

The rates of excitation and deexcitation by a single process are linked by the requirement of detailed balance (Mihalas 1978). For the average-atom model this can be written, for example for the case of two shells m and n, as

$$P_m^O \, Q_n^O \, R_{m \to n} = P_n^O \, Q_m^O \, R_{n \to m} \tag{7}$$

and for the case of one shell n and the continuum c as

$$Z^{*O} Q_n^O \, R_{c \to n} = P_n^O \, R_{n \to c} \tag{8}$$

where the superscript *0* represents the equilibrium values (after Lokke and Grasberger 1977). The equilibrium population P_n^O of shell n with energy E_n is simply the degeneracy of the level multiplied by the Fermi factor, which for a Maxwell-Boltzmann free electron distribution, with kT and E_n in units of keV is given by

$$P_n^O = \frac{2n^2}{1+\frac{317A}{\rho Z^{*o}}[kT]^{3/2}\exp(-E_n/kT)} \tag{9}$$

where Z^{*O} is the equilibrium value of Z^*

$$Z^{*O} = Z - \sum_{k=1}^{nmax} P_k^O \tag{10}$$

Consequently the deexcitation and excitation rates are related by

$$R_{n \to m} = \frac{P_m^O \, Q_n^O}{P_n^O \, Q_m^O} \, R_{m \to n}$$

$$= \frac{2m^2}{2n^2} \, \exp\left((E_m - E_n)/\, kT\right) R_{m \to n} \tag{11}$$

and the recombination and ionisation rates are related by

$$R_{c\to n} = \frac{P_n^O}{Z^{*O}\, Q_n^O} R_{n\to c}$$

$$= \frac{2n^2\rho}{317A(kT)^{3/2}} \exp(E_n / kT) R_{n\to c} \qquad (12)$$

The ionisation energy of a shell E_n is calculated using the hydrogen-like expression but replacing the nuclear charge by the screened hydrogenic charge appropriate to level n:

$$Z_n^* = Z - \sum_k \sigma_{nk} P_k \left[1 - \frac{\delta_{nk}}{2n^2}\right] \qquad (13)$$

(note Z_n^* is not the same as Z^* in equation (3)). Mayer (1947) gave expressions for and tabulated the screening constants σ_{nk} which express, for an electron in shell n, the fraction of the nuclear charge screened by an electron in shell k. The term involving δ_{nk} attempts to remove the non-physical self-screening from the expression. Since Mayer (1947), new screening constants have been tabulated by More (1982) and by Marchand, Caille and Lee (1990) by fitting to experimental data and data obtained from accurate computations. NIMP, however is not attempting spectroscopic accuracy and uses the original tabulation of Mayer (1947).

NIMP is intended for use with materials of a wide range of Z, and the effect of relativity must be included. This splits the degeneracy of a principal quantum shell into different levels of different total (sping plus orbital) angular momentum j (Bethe and Salpeter 1957). The Breit-Pauli expression is found to be sufficiently accurate for the model and gives, to first order in α^2

$$E_{n,k} = 0.0136 \frac{Z_n^{*2}}{n^2}\left[1 + \frac{\left[\alpha Z_n^*\right]^2}{n}\left[\frac{1}{|k|} - \frac{3}{4n}\right]\right] \qquad (14)$$

$$|k| = j + 1/2 = 1, \ldots\ldots, n$$

The ionisation energy E_n (keV) is taken as the average of the extreme values of the splitting

$$E_n = \frac{1}{2}\left(E_{n,1} + E_{n,n}\right) \qquad (15)$$

The collisional excitation rate used in NIMP is taken directly from Lokke and Grasberger (1977)

$$R^{c}_{m\to n} = 5.0x10^{-10} n_e f_{m\to n} \frac{e^{-(E_m - E_n)/kT}}{(E_m - E_n)(kT)^{1/2}} g_{mn}, \tag{16}$$

where n_e is the electron number density (cm^{-3})

$$n_e = \frac{Z^* \rho L}{A}, \tag{17}$$

and L is Avogadro's number. The excitation rate has dependences on temperature and energy expressed explicitly in equation (16) which are based on the work of Seaton (1962) who considered only electric-dipole allowed collisional excitation (hence the appearance of the absorption oscillator strength $f_{m\to n}$) and the Gaunt factor gmn attempts to improve the accuracy. It is given by (Lokke and Grasberger 1977)

$$g_{mn} = 0.19\left[1 + 0.9\left[1 + \frac{n(n-m)}{20}\left[1 - \left(1 - \frac{2}{Z}\right)U_{mn}\right]\right]e^{U_{mn}} E_1(U_{mn})\right] \tag{18}$$

where U_{mn} is simply

$$U_{mn} = \frac{E_m - E_n}{kT}, \tag{19}$$

and $E1(x)$ is the exponential integral. The collisional ionisation rate is also taken from Lokke and Grasberger (1977)

$$R^{c}_{n\to c} = 3.45x10^{-11} n_e \frac{(kT)^{1/2} e^{-E_n/kT}}{E_n^2} \Gamma_n \tag{20}$$

The dependences on electron number density, on temperature and ionisation energy are those which comes from the work of Seaton (1962), and the Gaunt factor Γ_n is given by (Lokke and Grasberger 1977)

$$\Gamma_n = 12.18\, e^{-n/(n+5)}(1 + 0.0335n)\left[1 - \frac{0.622}{Z} - \frac{0.0745}{Z^2}\right]\left[1 - e^{-U_n}\right] f(y) \tag{21}$$

where $f(y)$ is a polynomial of the form

$$f(y) = 0.23 + 0.046y + 0.1074\, y^2 - 0.0459\, y^3 - 0.01505\, y^4 \tag{22}$$

and y is given by

$$y = \log_{10}(U_n / 4), \tag{23}$$

with

$$U_n = E_n / kT \tag{24}$$

The radiative rates are not calculated in the same manner as Lokke and Grasberger (1977), who evaluate the rates in conjunction with a multigroup photon transport calculation; instead they are calculated using the radiation field which has been provided by the user as input data. The photoexcitation cross section (cm^2) is approximated as

$$\sigma_{m\to n}(\varepsilon) = 2.654x10^{-2} f_{m\to n}\phi_{m\to n}(\varepsilon) \tag{25}$$

where $f_{m\to n}$ is the absorption oscillator strength. and $\phi_{m\to n}$ is the line shape which we take here to be a delta function

$$\phi_{m\to n}(\varepsilon) = \delta(\varepsilon - \varepsilon_0) \tag{26}$$

and ε_0 is the transition energy (keV)

$$\varepsilon_0 = E_m - E_n. \tag{27}$$

The shell to shell oscillator strengths $f_{m\to n}$ involve an average over the initial substates of shell m and a sum over the substates of final shell n and are tabulated for $m,n < 5$. For all other transitions they are calculated from the semi-classical expression derived by Kramers (1923) (see Mihalas 1978).

$$f_{m\to n} = \frac{32}{3\pi\sqrt{3}}\left[\frac{1}{m^2} - \frac{1}{n^2}\right]^{-3}\left[\frac{1}{n^3 m^5}\right]. \tag{28}$$

For the photoionisation cross-section, the semi-classical bound-bound cross-section (equation 25) is extended into the continuum (as shown, for example by Mihalas 1978), giving

$$\sigma_{n\to c}\begin{cases} = \dfrac{1.99x10^{-23}Q_n^{*4}}{n^5\varepsilon^3} & \varepsilon \geq E_n \\ = 0 & \varepsilon < E_n \end{cases} \tag{29}$$

where ε is the photon energy (keV) and Q_n is a screened nuclear charge involving only 'inner' screening which is the appropriate form for photoionisation (Slater 1960)

$$Q_n^* = Z - \sum_{k=1}^{n} \sigma_{nk} P_k \left[1 - \frac{\delta_{nk}}{2}\right]\left[1 - \frac{\delta_{nk}}{2n^2}\right] \tag{30}$$

Introduction of these cross-sections into the standard expression for the photoexcitation rate (for example, Mihalas 1978) gives the following expressions for excitation and deexcitation

$$R^r_{m\to n} = 4.43x10^{13}\left(E_m - E_n\right)^2 f_{m\to n} f\left(E_m - E_n\right) \tag{31}$$

$$R^r_{n\to m} = \tag{32}$$

$$4.43x10^{13}\frac{P_m^O Q_n^O}{P_n^O Q_m^O}\left(E_m - E_n\right)^2 f_{m\to n}\left(1 + f\left(E_m - E_n\right)\right)\exp\left(-\left(E_m - E_n\right)/kT\right)$$

where $f(\varepsilon)$ is the number of photons per mode in the radiation field at energy ε (keV). For a Planck function at a radiation temperature equal to the material temperature

$$f(\varepsilon) = \frac{1}{e^{\varepsilon/kT} - 1} \tag{33}$$

where the temperature is also in keV, and in this case the rates are indeed in detailed balance:

$$R^r_{n\to m} = \frac{P_m^O Q_n^O}{P_n^O Q_m^O} R^r_{m\to n} \tag{34}$$

Introduction of the photoionisation cross-section (equation 29) into the standard expression for the photoionisation and radiative recombination rates (Mihalas 1978) gives for photoionisation

$$R^r_{n\to c} = 7.87x10^9 \frac{Q_n^{*4}}{n^5}\int_{E_n}^{\infty} \frac{1}{\varepsilon} f(\varepsilon) d\varepsilon, \tag{35}$$

and for radiative recombination

$$R^r_{c\to n} = 7.87x10^9\left[\frac{P^O_n}{Z^{*O}Q^O_n}\right]\frac{Q^{*4}_n}{n^5}\int_{E_n}^{\infty}\frac{1}{\varepsilon}\left(1+f(\varepsilon)\right)e^{-\varepsilon/kT}d\varepsilon \tag{36}$$

As with the case of photoexcitation and deexcitation, for a Planckian radiation field with a radiation temperature equal to the material temperature, detailed balance between the radiative recombination and photoionisation rates is found:

$$R^r_{c\to n} = \left[\frac{P^O_n}{Z^{*O}Q^O_n}\right]R^r_{n\to c}. \tag{37}$$

The present version of NIMP only allows for Planckian radiation fields (although the radiation temperature, T_r, need not be the same as the material temperature T_e). The integrals in equations (34) and (35) are evaluated with

$$f(\varepsilon) = \frac{1}{e^{\varepsilon/kT_r}-1} \tag{38}$$

by expanding as a sum of exponential integrals

$$\int_{E_n}^{\infty}\frac{1}{\varepsilon}\frac{1}{e^{\varepsilon/kT_r}-1}d\varepsilon = \sum_{m=1}^{\infty}E_1\left(\frac{mE_n}{kT_r}\right), \tag{39}$$

and

$$\int_{E_n}^{\infty}\frac{1}{\varepsilon}\left(1+\frac{1}{e_r^{\varepsilon/kT_r}-1}\right)e^{-\varepsilon/kT}d\varepsilon$$

$$= E_1\left(\frac{E_n}{kT}\right)+\sum_{m-1}^{\infty}E_1\left(E_n\left(\frac{m}{kT_r}+\frac{1}{kT}\right)\right) \tag{40}$$

Convergence of these sums is very slow for $E_n/kT \ll 1$, $E_n/kT_r \ll 1$. If the radiation field is included it is recommended that a relatively low value of *nmax* be used (typically 5 or 6) as using the highest value, *nmax* = 10, usually leads to the whole calculation being dominated by the evaluation of the expansions (39) and (40) for high n. Because the photoionisation rate is proportional to $\frac{1}{n^5}$ these terms are usually negligible.

The numerical solution of the *nmax* coupled non-linear differential equations for P_n (equation 4) proceeds as follows. We recast equation (4) as an implicit finite difference:

$$\frac{P_n^{new} - P_n^{old}}{\Delta t} = \left[1 - \frac{P_n^{new}}{2n^2}\right] A_n^{new} - P_n^{new} B_n^{new} \tag{41}$$

where the superscripts '*new*' and '*old*' refers to the quantity at the end or the beginning of the timestep Δt. A_n^{new} and B_n^{new} are A_n and B_n (equations 5 and 6) evaluated with shell populations P_n^{new} $(n = 1 \rightarrow nmax)$. The populations at the beginning of the timestep, P_n^{old} $(n = 1 \rightarrow nmax)$, are known. The right-hand-side of equation (41) is highly non-linear in P_n^{new} and an iterative solution method is used. Initially (k=1) the populations P_n^k are set to P_n^{old} and a guess at a solution to equation (41) is obtained from

$$\frac{P_n^{k+1} - P_n^{old}}{\Delta t} = \left[1 - \frac{P_n^{k+1}}{2n^2}\right] A_n^k - P_n^{k+1} B_n^k \tag{42}$$

which, when rearranged gives:

$$P_n^{k+1} = \frac{\left[P_n^{old} + A_n^k\right]\Delta t}{1 + \left[\frac{A_n^k}{2n^2} + B_n^k\right]\Delta t} \tag{43}$$

To damp oscillations a linear combination of the (k+1)th and the kth solution is taken

$$P_n^{k+1} \rightarrow \alpha\, P_n^{k+1} + (1-\alpha)\, P_n^k \tag{44}$$

From experience a value of α=0.5 has been adopted in NIMP. Following a similar procedure for each n $(n = 1 \rightarrow nmax)$, the next iterative cycle is started. If the difference in the sum of the populations between one such cycle and the next is smaller than *xtest*:

$$\sum_{n=1}^{nmax} \left| P_n^{k+1} - P_n^k \right| \le xtest \tag{45}$$

then the iteration is stopped and the procedure is judged to have converged at populations P_n^k which are a sufficiently good approximation to P_n^{new}, the actual solution of equation (41).

The accuracy of this numerical scheme depends on the timestep, Δt, but in the limit in which the rates into or out of the level are very fast, the scheme converges to the correct solution. If, for example the rate into the level is very fast, such that

$$A_n^k \Delta t >> B_n^k \Delta t$$
$$A_n^k \Delta t >> 2n^2 \tag{46}$$

then the scheme will converge on the solution of a full shell, $P_n^{new} = 2n^2$, and the shell will have filled after one timestep. Alternatively, if the rate out of the level is very fast

$$B_n^k \Delta t >> A_n^k \Delta t$$
$$B_n^k \Delta t >> 2n^2 \tag{47}$$

then the scheme converges to the solution of an empty shell $P_n^{new} = 0$, and the shell will empty in one timestep.

The upwards and downwards rates between any two levels are related by detailed balance, and because we have assumed that the free electrons are non-degenerate, numerical problems arise when the plasma is partially-degenerate (typically at low temperature and high-density, such as occurs in the initial heating of a solid target by a high-power laser). Under these conditions the rate equations predict over-population of the bound levels. Introduction of the effects of degeneracy into the non-LTE average-atom model is possible in an approximate way (Pollack 1990), but for most applications of NIMP the plasma is non-degenerate at the time of interest and so we use a simple numerical device to avoid the problem. In the iterative solution, if

$$\sum_{n=1}^{nmax} P_n^k > Z - 1 \tag{48}$$

then the populations P_n^{new} $(n = 1 \rightarrow nmax)$ are reset filling the shells in order of increasing energy such that

$$\sum_{n=1}^{nmax} P_n^{new} = Z - 1 \tag{49}$$

The populations are also reset in this way if the number of iterations exceeds 600. This is set to be sufficiently large that if it is exceeded our experience is that convergence is unlikely given a larger number of iterations.

The numerical solution of the rate equations produces $P_n(t)$ and $Z^*(t)$ at each timestep. Printing of these quantities, together with $P_n^O(t)$ and $Z^{*O}(t)$ takes place every *nstep* timesteps. For comparison with experiment, we require, not shell populations, but number densities of particular ionic states. In the X-ray laser community this problem has been solved by using the non-LTE average-atom calculation (in essence that described above) interfaced with a radiation-hydrodynamics calculation to give an estimate of the hydrodynamic evolution. Following this a separate calculation is performed to solve the time-evolution of the detailed ionic states which post-processes the hydrodynamic information (for example see Rosen et al 1988). In NIMP we do not attempt to solve the coupled rate equations for the detailed states, only for the shell populations and we reconstruct the populations of the detailed states, or groups of states, using the shell populations alone. To do this, we assume that the electrons are not statistically correlated (the fundamental assumption of the average-atom model) and then, using the binomial theorem, the probability of finding a 'configuration'

$$\alpha : \{k_1, k_2 ....., k_{nmax}\}$$

where k_n is the integral population of principal quantum shell n, is

$$P(\alpha) = \prod_{n=1}^{nmax} \frac{2n^2!}{k_n!(2n^2 - k_n)!} \left[\frac{P_n}{2n^2}\right]^{k_n} \left[1 - \frac{P_n}{2n^2}\right]^{2n^2 - k_n} \tag{50}$$

In general the configuration α encompasses many ionic states. For example, the configuration {2,2,0,....} (i.e. two electrons in the K-shell and two in the L-shell) comprises, in LS-coupling, the following ionic states

$1s^2 2s^2 \quad {}^1S_0$

$1s^2 2s2p \; {}^1P_1 \, , {}^3P_{2,1,0}$

$1s^2 2p^2 \quad {}^1S_0 \, , {}^1D_2 \, , {}^3P_{2,1,0}$

The total degeneracy of the configuration α is

$$G(\alpha) = \prod_{n=1}^{nmax} \frac{2n^2!}{k_n!(2n^2 - k_n)!}, \tag{51}$$

which in this case is 32 (in agreement with adding the degeneracies of each individual ionic state). The use of equation (50) does not, by itself, allow the calculation of the fraction of ions in, for example, the ionic state $1s^2 2s2p\ ^1P_1$. For many applications the level of detail provided by equation (50) is however sufficient. This is particularly true of open M-, N- .... shells where the number of ionic states resulting from one configuration α can be so large that it is usually only practical to estimate the relative fractions of ions with different numbers of electrons in a principal quantum shell. Equation (50) provides just this level of resolution.

If the ionic states resulting from a single configuration α are statistically populated (this can occur, for example, when the levels are in equilibrium with one another and the typical energy splitting is less than kT), then the fraction S of ions in a particular ionic state of total angular momentum J is

$$S = \frac{2J+1}{G(\alpha)} P(\alpha). \tag{52}$$

However, it is usually not worthwhile going to the level of detail given by equation (52), either because the assumption of statistically populated levels is questionable, or, and this is particularly serious in practise, because the number of states can become very large (particularly for open M-, N- ..... shells).

3. Examples of the use of NIMP

3.1 Steady-state ion-stage distributions

To begin this section on applications, we compare the predictions of NIMP with those of other published data. Lee (1987) considered an optically thin selenium plasma at an electron temperature of 1000eV and an electron density of $5x10^{20}\,cm^{-3}$. Lee (1987) calculated, using a model which explicitly considered different ionic states, the distribution of ion stages in the steady-state. Figure 3 shows a comparison between the distribution calculated by Lee (1987) and the steady-state result from NIMP, obtained by continuing the calculation until $dP_n / dt = 0\ (n = 1 \rightarrow nmax)$. The fraction of, for example, C-like ions is calculated as $P(\alpha)$ where

α : {2,4,0,.....}

This includes all the ionic states arising from the configurations $1s^2 2s^2 2p^2, 1s^2 2s 2p^3$ and $1s^2 2p^4$. The agreement is very (and probably fortuitously) good, but indicates that the use of the binomial theorem to calculate the populations of ionic states from shell populations can give accurate results.

It should be noted, however, that NIMP does not include at present any description of dielectronic recombination. Lee (1987) estimates that inclusion of this effect for the selenium plasma just considered reduces the average ionisation stage by approximately two. Dielectronic recombination becomes less important in relation to three body recombination as the density increases. This should be borne in mind when using NIMP at low densities. An approximate prescription of dielectronic recombination has been included in special versions of NIMP.

3.2 The effect of an ambient radiation field on the state of excitation and ionisation in a plasma

The direct irradiation of a solid target by a long-pulse (nsec) high-power laser beam leads to the production of a plasma which has high spatial gradients of both electron temperature and density. For meaningful measurement of plasma properties it is necessary to produce a plasma of uniform temperature and density. This has been achieved experimentally by the use of indirect heating of a sample of material using X-rays produced by a separate laser-produced plasma. A typical experimental arrangement is shown in figure 4 in which the high-power laser is focussed onto a thin foil of high-Z material (typically gold) supported on

a thin plastic substrate. The X-ray conversion efficiency in the gold is very high (typically 50%) and the flux of X-rays heats the plastic allowing good transmission. However the laser light does not penetrate the foil and the sample is only heated by the soft X-ray flux. The long mean free path of X-ray photons, together with the tamping of the sample between two layers of plastic ensures that the gradients in temperature and density through the sample are low, although gradients do exist across the foil, the side closest to the X-ray source having the highest temperature. Several experiments have been performed in which the absorption spectrum of the sample is taken using the point-projection backlighting technique (Davidson et al 1988,1989, Foster et al 1991). The backlighting target is irradiated at some time after the start of the main pulse to allow for the sample to decompress. Absorption spectra have been recorded, typically at a temperature of less than 100eV and typical densities of 10^{-2} x solid. Experiments have so far measured the absorption and thereby the opacity of heated samples of aluminium and germanium. The experimental measurement has in each case been compared to calculations of the opacity in which LTE has been assumed to hold. In this section we use the NIMP code to investigate the state of excitation/ionisation in both aluminium and germanium experiments and to ascertain the effect of the ambient radiation field on the plasma. Although we could investigate the problem by calculating the time-dependent excitation and ionisation of the plasma using the time-histories of the temperature, density and radiation field, the plasma is close to a steady-state and for ease of presentation, results from steady-state calculations (performed by running the time-dependent calculation with fixed temperature and density until there is no change in the population, $dP_n / dt = 0,\ n = 1 \rightarrow nmax$) are presented here. Figures 5(a) and (b) show the steady-state populations of the open shells for aluminium and germanium respectively. For the aluminium case, the absorption spectrum was taken at a temperature of 40eV and a density ρ_{expt} = 0.013gcm^{-3}. Under these conditions open L-shell aluminium ions are found and figure 5(a) shows the steady-state population of the L-shell, P_2, calculated by NIMP at 40eV and $\rho = \rho_{expt} / 10$, $\rho = \rho_{expt}$ and $\rho = 10\rho_{expt}$ with no radiation field $(T_r = 0)$. In addition, the figure shows P_2^Q, the values of the populations from equation (9). The figure also shows the effect on the populations of an ambient Planckian radiation field $(T_r = T_e)$. With this radiation field $P_2 = P_2^Q$ showing that the steady-state L-shell population is in LTE. Figure 5(b) shows the equivalent calculation for germanium at a temperature of 76eV and a density ρ_{expt} = 0.054gcm^{-3}. Under these conditions open M-shell germanium ions are found and figure 5(b) shows the steady-state population of the M-shell, P_3, calculated by NIMP at 76eV and, as for aluminium, $\rho = \rho_{expt} 10$, $\rho = \rho_{expt}$ and $\rho = 10\rho_{expt}$. P_3^Q, calculated from equation (9) is also shown. As with aluminium, the presence of the ambient Planckian radiation field pumps the steady-state populations into LTE and $P_3 = P_3^Q$.

For both the aluminium and germanium experiments, the density of the material was sufficiently great that collisional rates dominate radiative rates for the open shell and at $\rho = \rho_{expt}$, without a radiation field, the populations are close to the LTE values. At $\rho = 10\rho_{expt}$, the non-LTE and LTE populations are almost identical, whereas at $\rho = \rho_{expt}/10$ this is not the case and the populations depart markedly from the LTE values. However, for all densities, the introduction of the radiation field pumps the material into exact thermodynamic equilibrium. This demonstrates another useful effect of employing soft X-rays to heat the sample: the radiation field, if it is truly Planckian, will ensure LTE even when the plasma density is low enough that collisional rates do not dominate radiative rates.

Figures 5(a) and (b) illustrate an important yet difficult aspect of the average-atom model. It appears from these figures that for a given n there are two P_n^O values, one with and one without the Planckian radiation field. How can this be the case; surely there can be only one LTE solution for a given temperature and density? In fact there is only one LTE solution and this is the P_n^O value for the Planckian radiation field with $T_r = T_e$. The fact that P_n^0 varies with T_r can be seen by studying equation (9) which defines P_n^O. The energy, E_n, in that equation is the non-LTE energy appropriate for the populations P_n $(n = 1 \rightarrow n\max)$. The true equilibrium population of shell n would be given by equation (9) with E_n replaced by the LTE energy which occurs when $T_r = T_e$. P_n^O is defined by equation (9) to be the correct population to appear in the equations describing detailed balance (equations 11 and 12).

Figures 6(a) and (b) show the steady-state populations of shells of higher principal quantum number for aluminium and germanium respectively. Values are shown for the case of no radiation field $(T_r = 0)$ and for the case of a Planckian radiation field with $T_r = T_e$ (which is the LTE value). In each case the steady-state populations calculated with no radiation field are very close to the values calculated with the Planckian radiation field. The difference between this case and that shown in figure 5 is because the collisional rates are higher and the radiative rates lower for higher principal quantum shells.

So far in this section we have looked at the average populations of the shells, but if we now use these populations to calculate the distribution of ionization in the same way as was done in the previous section, we come across a severe problem with the use of equation (50). It is best illustrated for a plasma in LTE, although similar effects occur away from equilibrium. Taking the experimental conditions of 40 eV and $0.013 gcm^{-3}$ for the aluminium plasma, using the LTE average populations from NIMP (by taking a Planckian radiation field with $T_r = T_e$) gives the distribution of ionization shown in Figure 7. As before we calculate, for

example, the fraction of C-like aluminium to be $P(\alpha)$ with $\alpha:\{2,4,0,.....\}$. Comparison is made in figure 7 with an independent calculation of the distribution of ionization including the same ionic states but using much more detailed and accurate atomic physics, together with a calculation of states using the Saha/Boltzmann equations (Rose 1992). What is noticeable is that although NIMP predicts almost the same average degree of ionization, the width of the distribution is much greater for NIMP and leads to serious error. That error can be traced to the assumption in the use of equation (50) that the electrons are uncorrelated. For the case of thermodynamic equilibrium, the parameter which describes the degree of correlation is *H/kT* where *H* is a measure of the interelectron interaction energy between electrons in the open shell. When $H/kT \geq 1$ bound electron populations become correlated and the use of equation (50) leads to a distribution of ionization stages which is too wide. There is an exact correspondence between *H/kT* and the strong-coupling parameter for free particles in a plasma, Γ. Γ is the ratio of the electrostatic interaction of *kT* and for $\Gamma \geq 1$ the free particle motion is correlated. Indeed *H/kT* is the strong-coupling parameter for bound electrons. For the aluminium plasma at 40 eV, $H/kT \sim 1$. Whereas *H/kT* is a measure of the correlation between bound electrons for a plasma in thermal equilibrium the correlation for non-LTE systems cannot be described by a single parameter (see More, Zimmerman and Zinaman 1988).

3.3 Atomic kinetics with short-pulse lasers

The development of short-pulse (picosecond or sub-picosecond) high-power lasers has led to many possible applications which are currently being explored. If a prepulse-free short-pulse (preferably sub-picosecond) laser is incident upon a solid target, experimental evidence and numerical simulation both suggest that a hot (several hundred eV up to 1 keV), dense (solid density or just below) plasma is produced transiently at the surface. Such hot, dense plasmas are interesting for study in their own right or for applications such as short-pulse X-ray sources. In either case, the study of the time-dependent ionisation characteristics of such plasmas is of great current interest and provides a good example of the utility of the NIMP code. To investigate ionisation on such short time-scales we use a model calculation in which the temperature, density and radiation field are fixed throughout the calculation and the ionisation of a low (Al), medium (Fe) and high-Z (Sn) material is followed. In the calculations reported here, the density is $1 gcm^{-3}$ and three different temperatures are investigated (100eV, 500eV, 1000eV) both with and without a Planckian radiation field characterised by a temperature equal to that of the material. The number of shells to be included in the calculation, *nmax*, was estimated by a separate calculation to be 6. The sensitivity of the NIMP calculation to the value of *nmax* can be seen by comparing a particular case of Al at 500eV, where using *nmax*=6 results in a slightly more rapid

ionisation than for *nmax*=3 because the number of levels available for excitation and thus the number of routes for ionisation is increased. The steady-state Z^* increased for *nmax*=3 (by 5%) because the number of available states is less than for *nmax*=6.

To assess any effect on the solutions of the initial conditions, a calculation was performed for Al at 500eV with shells filled at t=0 from the lowest energy level in order of increasing energy but with the total number of electrons given by *Z-3* and not *Z-1* (as is the default case). The two calculations were almost indistinguishable after 10^{-14} sec.

The timestep Δt was held constant throughout the calculations at 10^{-16}sec and was chosen such that $\Delta t \leq 1/$(maximum rate). This was found to be sufficiently accurate in that a time step of 10^{-17}sec reproduced the results of all calculations almost exactly, except at very early times (<10^{-14} sec).

Figures 8(a), (b) and (c) show Z^* as function of time for Al, Fe and Sn respectively. As can be seen, for these conditions Z^* is dominated by collisions and the presence of the radiation field has a small effect, increasing the value of Z^* no more than about 10% at any time. As expected, the effect is greatest for the largest radiation fields (1000eV).

These predictions have been made assuming a Maxwellian distribution of particle energies. To assess the validity of this assumption we define for the free electrons an average inelastic collision time τ_i, and a characteristic thermalisation time τ_t. A departure from a Maxwellian distribution would be expected due to the inelastic processes if $\tau_i \leq \tau_t . \tau_t$ can be estimated from the expression given by Spitzer (1956)

$$\tau_t = \frac{5x10^{-15}(kT_e)^{3/2} A}{\rho Z^*}. \qquad (53)$$

where kT_e is the electron temperature in keV and ρ is the material density in gcm^{-3}. As the ionisation progresses, the values of τ_t decrease as the electron density increases. During the period of ionisation, the average inelastic collision time can be approximated as $Z^*/(dZ^*/dt)$ which is the average time for an electron to cause a single ionisation of an ion. From figures 8(a)-(c) it may be seen that $Z^*/(dZ^*/dt)$ decreases with increasing temperature but increases as the ionisation progresses. Therefore the ratio $\Gamma = \tau_t / \tau_i$ is expected to be largest for high temperatures and early times. For example at 100eV, at early times, Γ varies between approximately 0.1 and 1.0. The ratio rises rapidly, reaching approximately 10 between 5 and 20 fsec. Thus departures from a Maxwellian distribution are expected to occur, particularly

at early times and high temperatures. At later times, the condition for a Maxwellian distribution appears to be satisfied.

In summary, NIMP has been used to estimate the time-dependant ionisation of aluminium, iron and tin under plasma conditions thought to be typical of those produced under short-pulse laser irradiation. Particularly for the cases of iron and tin, constructing detailed models which span ionisation stages from neutral to many times ionised, which would be needed to follow the ionisation evolution on such short time-scales, would involve a prohibitively large amount of atomic data. The non-LTE average-atom model NIMP is therefore particularly useful in this case, although the model does make assumptions about the number of bound shells and the free electron energy distribution which are open to question.

3.4 Population inversion in a recombining plasma

Amplified spontaneous emission (ASE) in the XUV spectral region was first demonstrated between levels of Ne-like selenium ions in a high power laser produced plasma (Matthews et al 1985). The two levels were from the configurations $1s^2 2s^2 2p^5 3p$ and $1s^2 2s^2 2p^5 3s$ and the lasing transitions are between levels of the same principal quantum number ($\Delta n = 0$). Although it may, at first sight, appear possible to estimate the population of the upper and lower levels with NIMP using equation (52), the assumption that the states are statistically populated does not allow the possibility of selective pumping and NIMP, as it stands, is not able to give any value for the population inversion in such a scheme. Another method of pumping a population inversion in a laser-produced plasma, recombination pumping, was demonstrated experimentally soon after the collisional scheme. In the original experiments (Chenais-Popovics et al 1987), a thin carbon fibre, typically 7μm diameter and up to 1cm long, was irradiated by several overlapping beams in line focus. This produced an expanding cylindrical plasma which is initially nearly fully stripped. As the plasma expands and cools recombination takes place, preferentially through the upper levels and populates the upper lasing level: $n=3$ in H-like carbon. In addition, a fast radiative decay from $n=2$ to $n=1$ in H-like carbon (Lyman α) empties the lower lasing level, producing a population inversion between $n=3$ and $n=2$ (Balmer α). Because on this occasion the lasing transition is between levels of different principal quantum number, NIMP can calculate the value of the population inversion. The different levels of H-like carbon correspond to configurations as follows:

α : {1,0,0,0,0....} $(n=1)$
β : {0,1,0,0,0....} $(n=2)$
γ : {0,0,1,0,0....} $(n=3)$
δ : {0,0,0,1,0....} $(n=4)$

The expression for the degeneracies $G(\alpha)$, $G(\beta)$ (equation 51) reduce as expected, to $2n^2$, whilst the probabilities $P(\alpha)$, $P(\beta)$, are given by equation (50). The fractional population inversion between $n=3$ and $n=2$, Δ, is given by

$$\Delta = \frac{P(\gamma)}{G(\gamma)} - \frac{P(\beta)}{G(\beta)}.$$

For the plasma to exhibit gain on Balmer α, $\Delta>0$.

We have obtained typical time histories of both electron temperature and density for a C-fibre recombination XUV laser experiment (derived from the work of Jacoby et al 1982) and these are shown in figure 9. Using these values in NIMP we have calculated the time history of the reduced populations $P(\alpha)/G(\alpha)$, $P(\beta)/G(\beta)$, and the population inversion Δ. These values are plotted in figure 10. Indeed $\Delta > 0$ for later times in the calculation showing that such a plasma would exhibit gain.

NIMP, coupled to the hydrodynamics code MEDUSA, has been used extensively to calculate the gain in H-like recombination laser schemes (Pert and Rose 1990). In these calculations several extra effects are included, such as the effect of line-trapping on the 2-1 line and photon transport along the axis of the plasma amplifier.

4. Input and output

NIMP is written in FORTRAN and has been checked extensively for coding errors using a static code analyser (FORCHECK, Leiden University, Netherlands) and has been compiled successfully with no errors on a number of different compilers on a range of platforms from PCs to supercomputers. The code can be obtained from the author by contacting him directly (s.j.rose@rl.ac.uk).

The code takes in data on stream 1 and writes the results to stream 6. A summary of configuration fractions at different times is written to stream 10. As an example we show the input data and the output data from the calculation of the population inversion in a carbon plasma (section 3.4).

Input data

The input data is read in in free format with read statements corresponding to the following lines in the input data file:

Input data file format

Line 1 read(1,*) z,a

z is the nuclear charge
($1.0 \leq z \leq 92.0$)
a is the atomic weight
($1.0 \leq a \leq 238.0$)

Line 2 read(1,*) iradf1

iradf1 is the flag which determines whether a radiation field is to be included
iradf1=0 - no field
iradf1≠0 - Planckian field

Line 3 read(1,*) nmax

nmax is the number of principal quantum shells to be considered in the calculation
($1 \leq nmax \leq 10$)

Line 4 read(1,*) xtest

xtest is the accuracy value used in the numerical solution of the rate equations and in the solution of the LTE population equations
($0.1 \leq$ xtest ≤ 0.0000001)

Line 5 read(1,*) tstep,nstepm

tstep is the timestep used in the solution of the rate equations
($1.0e\text{-}20 \leq$ tstep $\leq 1.0e\text{-}06$)
nstepm is the number of timesteps used in the rate equation calculations
($0 \leq$ nstepm ≤ 1000000)

Line 6 read(1,*) iprnt

iprnt is the number of timesteps between printing

Line 7 read(1,*) nconf

nconf is the number of 'principal quantum number configurations' to be considered
($0 \leq$ nconf ≤ 10)

Line 8 - (7+nconf)
kk=1,nconf read(1,*) (nph(kkk,kk) kkk=1,nmax)

nph(kkk,kk) is the occupancy of principal quantum shell kkk in configuration kk
($0 \leq$ nph(kkk,kk) $\leq (2kkk^2)$)

Line 8 + nconf
read(1,*) nd

nd is the number of times for which data will be provided
($2 \leq$ nd ≤ 100)

Line (9+nconf) - (8+nconf+nd)
kk=1,nd read(1,*) timnsd(kk),rhd(kk),teevd(kk),trevd(kk)

timnsd(kk) is the time in nsec

rhd(kk) is the density in g/cc
teevd(kk) is the electron temperature in eV
trevd(kk) is the radiation temperature in eV
(timnsd,rhd,teevd,trevd >0)

An example of an input data file, for the case of the recombining carbon plasma is given below

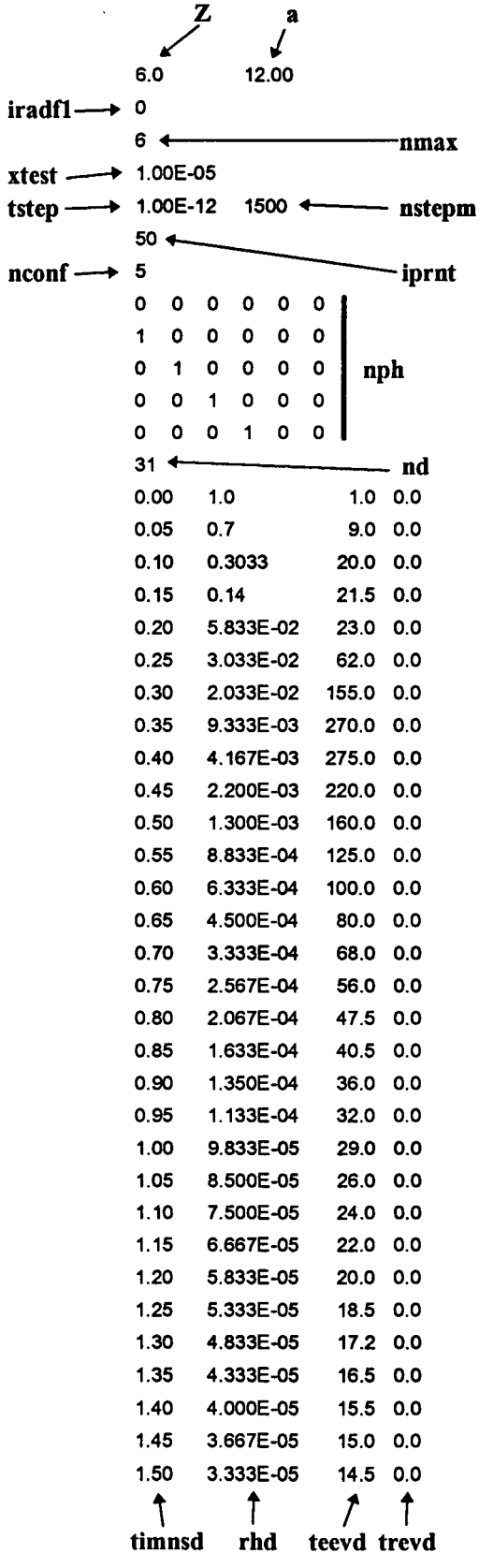

Output data file format

The main output data is written to stream 6, an example of which, again for the case of the recombining carbon plasma is given below. The printing occurs every iprnt timesteps and one such set of printing is annotated in detail below

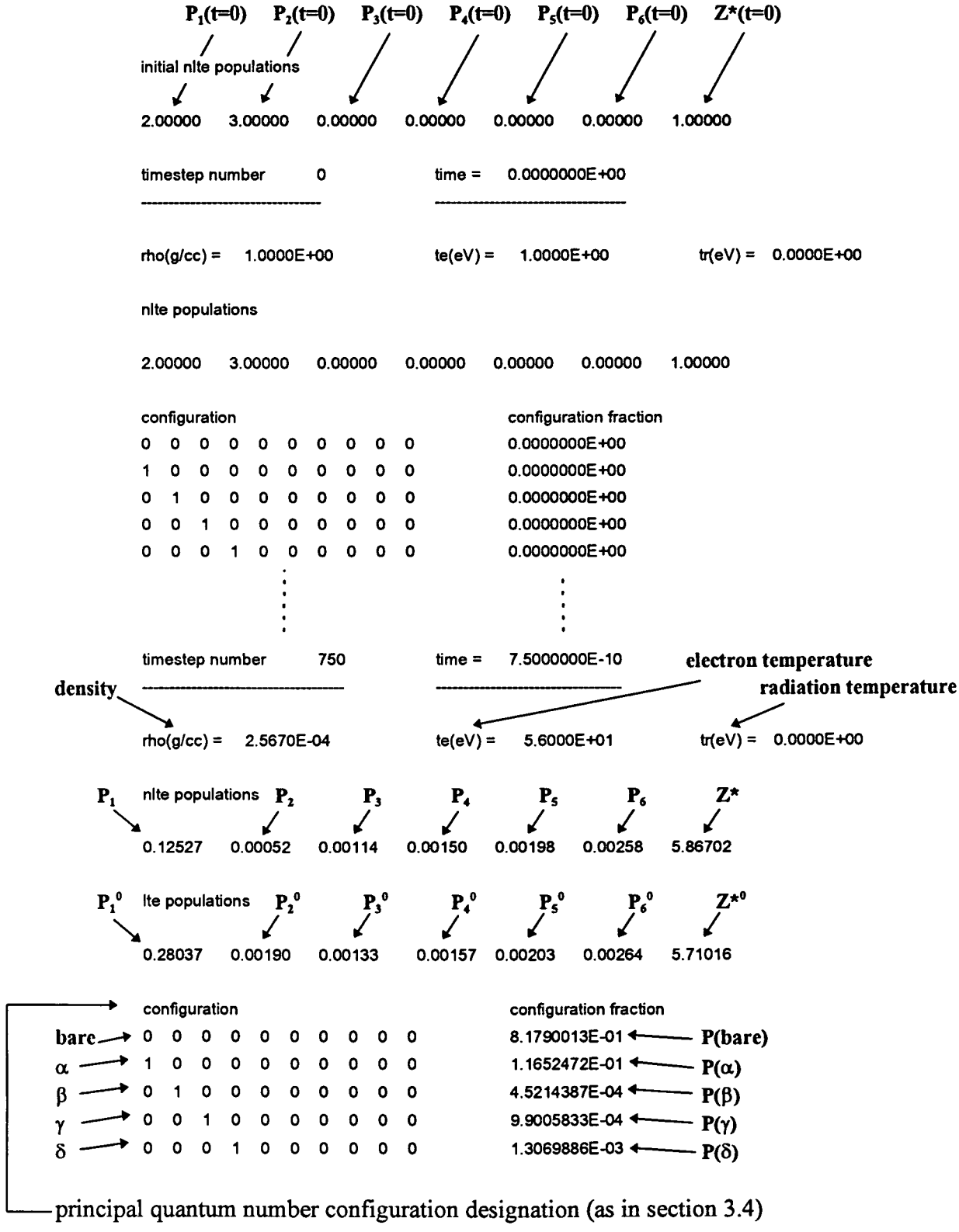

A summary of the configuration fractions at each iprnt timesteps is written in a line, starting with the time, to stream 10. An annotated example of this output file, again for the example of a recombining carbon plasma is given below.

time(sec)	P(bare)	P(α)	P(β)	P(γ)	P(δ)
0.000E+00	0.000E+00	0.000E+00	0.000E+00	0.000E+00	0.000E+00
5.000E-11	6.358E-30	8.811E-16	2.263E-29	3.516E-30	0.000E+00
1.000E-10	2.484E-14	6.845E-08	2.067E-14	1.130E-14	1.284E-14
1.500E-10	5.889E-13	3.428E-07	3.426E-13	2.160E-13	2.821E-13
2.000E-10	9.663E-01	2.102E-06	4.164E-12	2.653E-12	3.371E-12
2.500E-10	1.057E-01	1.143E-01	4.601E-04	5.720E-04	8.416E-04
3.000E-10	8.164E-01	7.467E-02	7.697E-03	1.084E-02	1.653E-02
3.500E-10	9.699E-01	8.418E-03	1.427E-03	2.342E-03	3.793E-03
4.000E-10	9.837E-01	6.796E-03	6.578E-04	1.032E-03	1.668E-03
4.500E-10	9.825E-01	1.038E-02	5.415E-04	7.894E-04	1.250E-03
5.000E-10	9.734E-01	1.988E-02	5.530E-04	7.861E-04	1.207E-03
5.500E-10	9.579E-01	3.478E-02	5.592E-04	8.110E-04	1.213E-03
6.000E-10	9.382E-01	5.388E-02	5.439E-04	8.518E-04	1.241E-03
6.500E-10	9.159E-01	7.520E-02	5.101E-04	9.000E-04	1.271E-03
7.000E-10	8.938E-01	9.635E-02	4.560E-04	8.981E-04	1.235E-03
7.500E-10	8.719E-01	1.165E-01	4.521E-04	9.901E-04	1.307E-03
8.000E-10	8.492E-01	1.370E-01	4.652E-04	1.105E-03	1.399E-03
8.500E-10	8.262E-01	1.576E-01	4.648E-04	1.211E-03	1.465E-03
9.000E-10	8.036E-01	1.776E-01	4.519E-04	1.271E-03	1.486E-03
9.500E-10	7.814E-01	1.969E-01	4.467E-04	1.350E-03	1.521E-03
1.000E-09	7.592E-01	2.158E-02	4.461E-04	1.426E-03	1.555E-03
1.050E-09	7.367E-01	2.344E-01	4.537E-04	1.536E-03	1.613E-03
1.100E-09	7.141E-01	2.530E-01	4.477E-04	1.588E-03	1.621E-03
1.150E-09	6.917E-01	2.709E-01	4.481E-04	1.659E-03	1.644E-03
1.200E-09	6.690E-01	2.886E-01	4.486E-04	1.743E-03	1.670E-03
1.250E-09	6.460E-01	3.060E-01	4.585E-04	1.832E-03	1.703E-03
1.300E-09	6.228E-01	3.232E-01	4.592E-04	1.888E-03	1.708E-03
1.350E-09	6.008E-01	3.395E-01	4.212E-04	1.784E-03	1.601E-03
1.400E-09	5.800E-01	3.541E-01	4.077E-04	1.769E-03	1.563E-03
1.450E-09	5.603E-01	3.679E-01	3.792E-04	1.678E-03	1.474E-03
1.500E-09	5.424E-01	3.802E-01	3.406E-04	1.546E-03	1.361E-03

5. Conclusions

NIMP is a simple model which allows one to follow the time evolution of the excitation and ionisation in a plasma for which the time-history of the plasma conditions have been supplied as data. Although it uses the average-atom model, by making use of the assumption that the bound electron populations are not statistically correlated the probability of finding a specific electronic bound-electron configuration in the plasma can be calculated. Comparison with more detailed models shows good agreement and the code has been used extensively to analyse high-power laser experiments in a number of different laboratories.

It is perhaps appropriate at this point to list some enhancements to the code which, it is envisaged may be incorporated in future versions. The code only allows single materials to be used and could be enhanced to allow mixtures. The effects of free electron degeneracy are not included; for degenerate plasmas changes need to be made to the calculation of one electron LTE populations as well as electron collisional rates. The effect of continuum lowering is also not included, although the user has the option of picking a maximum principal quantum shell for the entire calculation. These and other enhancements may be included in future versions.

We hope that you enjoy using NIMP and that it is useful to you.

6. Acknowledgments

The author would like to thank Mr. P. Jobbins for his efforts in helping compile this report.

Figure Captions

Figure 1. Schematic diagram showing the collisional rates affecting the population of shell *n*.

Figure 2. As figure 1, but showing both spontaneous and stimulated radiative rates.

Figure 3. A comparison of the distribution of ionisation calculated by NIMP (——) and by the detailed model of Lee (1987) (-------) for the case of an optically thin selenium plasma at an electron temperature of 1000eV and and electron density of 5 x 10^{20}cm^{-3}. For the NIMP calculation this corresponds to a density of 2.5 x 10^{-3} gcm^{-3}.

Figure 4. Schematic diagram of the experimental arrangement of soft X-ray heating in absorption experiments.

Figure 5(a). Density dependence of steady-state aluminium L-shell populations at T_e=*40eV*.
Figure 5(b). Density dependence of steady-state germanium M-shell populations at T_e=*76eV*.

Figure 6(a). Density dependence of the *n=3* and *n=4* shell populations in aluminium at T_e=*40eV*.
Figure 6(b). Density dependence of the *n=4* and *n=5* shell populations in germanium at T_e=*76eV*.

Figure 7 A comparison of the distribution of ionization calculated by NIMP (——) and by the detailed model of Rose (1992) (------) for an aluminium plasma at 40 eV and 0.013 gcm^{-3} in LTE.

Figure 8(a). The average degree of ionisation Z^* calculated as a function of time for an aluminium plasma at 1 gcm^{-3} and with electron temperatures of 100eV, 500eV and 1000eV. The curves marked ——— indicate no ambient radiation field and those marked ----- indicate a Planckian radiation field characterised by the material temperature.
Figure 8(b). As figure 8(a), but for iron.
Figure 8(c). As figure 8(a), but for tin.

Figure 9(a). Time dependence of the density, ρ and (b) of the electron temperature, T_e, in an expanding carbon plasma.

Figure 10(a). Time dependence of the reduced populations of the *n=1,2,3* and *4* levels and (b) of the reduced population inversion on Balmer α, Δ, in H-like carbon.

References

H A Bethe and E E Slapeter, "Quantum Mechanics of One- and Two-Electron Atoms", Springer-Verlag, Berlin (1957).

C Chenais-Popovics et al, Phys. Rev. Letts., **59**, 2160 (1987).

S J Davidson et al, Appl. Phys. Letts., **60**, 2034 (1988).

S J Davidson et al, in 'Laser Interactions with Matter', edited by G Verlarde, E Minguez and J M Perlado, World Scientific (1989).

J Foster et al, Phys. Rev. Letts., **67**, 3255 (1991)

W H Grasberger, Lawrence Livermore National Laboratory internal report UCRL-12408 (1965).

W H Grasberger, Lawrence Livermore National Laboratory internal report UCRL-50135 (1966).

D Jacoby et al, J. Phys. B: Atom. Molec. Phys., **15**, 3557 (1982).

H Kramers, Phil. Mag, **46**, 836 (1923).

Y T Lee, JQSRT, **38**, 131 (1987).

W A Lokke and W H Grasberger, Lawrence Livermore National Laboratory internal report UCRL-52276 (1977).

R Marchand, S Caille and Y T Lee, JQSRT, **43**, 149 (1990).

D L Matthews et al, Phys. Rev. Letts., **54**, 110 (1985).

H Mayer, Los Alamos National Laboratory internal report LA-647 (1947).

D Mihalas, 'Stellar Atmospheres', second edition, W H Freeman and Co, San Francisco (1978).

R M More, JQSRT, **27**, 345 (1982).

R M More, G B Zimmerman and Z Zinaman in "Atomic Processes in Plasmas", AIP Conference Proceedings, **168**, AIP, New York p33 (1988).

G J Pert and S J Rose Appl. Phys. B, **50**, 307 (1990).

M S Rosen et al, in "Atomic Processes in Plasmas", AIP Conference Proceedings **168**, AIP, New York, p102 (1988).

M J Seaton in "Atomic and Molecular Processes", edited by D R Bates, (Academic Press, New York), p 375, (1962).

J C Slater, 'Quantum Theory of Atomic Structure', volume 1, p227, McGraw Hill (1960).

H Van Regemorter, Ap.J., **136**, 906 (1962).

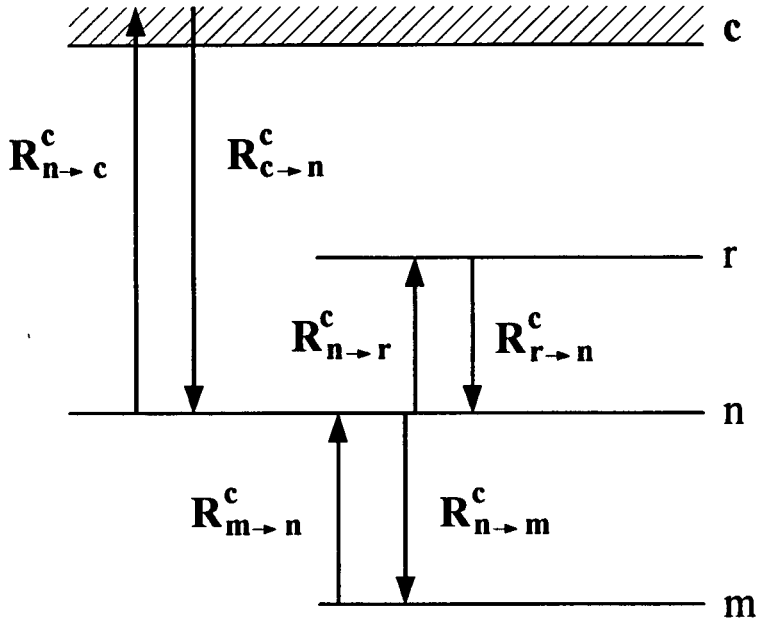

collisional rates

Figure 1

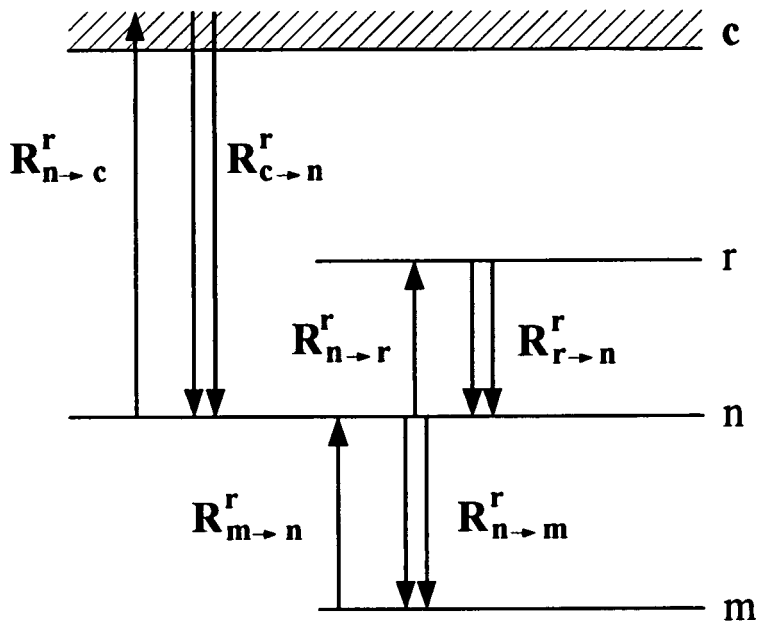

stimulated and spontaneous
radiative rates

Figure 2

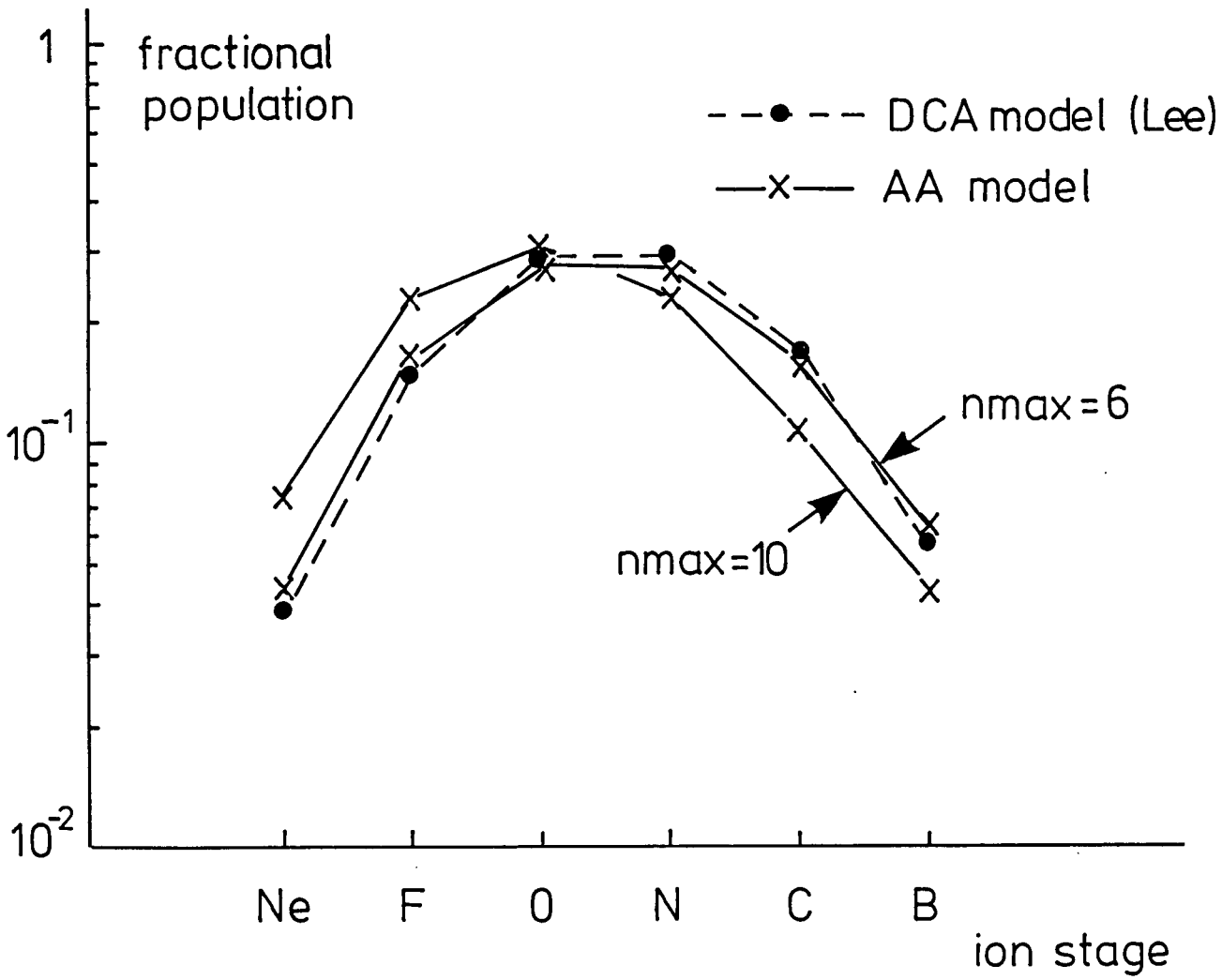
1
fractional
population
DCA model (Lee)
AA model
nmax=6
nmax=10
10^{-1}
10^{-2}
Ne
F
O
N
C
B
ion stage

Figure 3

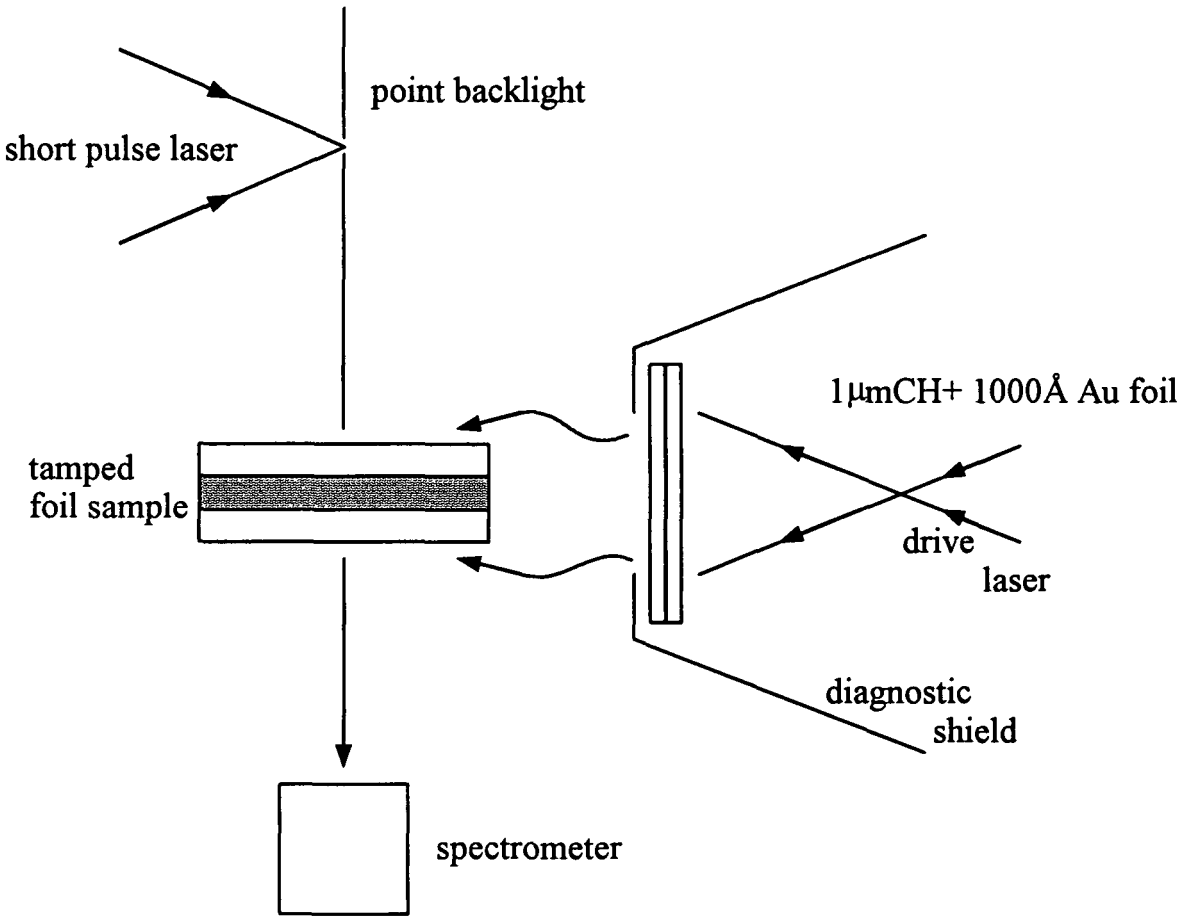
point backlight
short pulse laser
1μmCH+ 1000Å Au foil
tamped
foil sample
drive
laser
diagnostic
shield
spectrometer

Figure 4

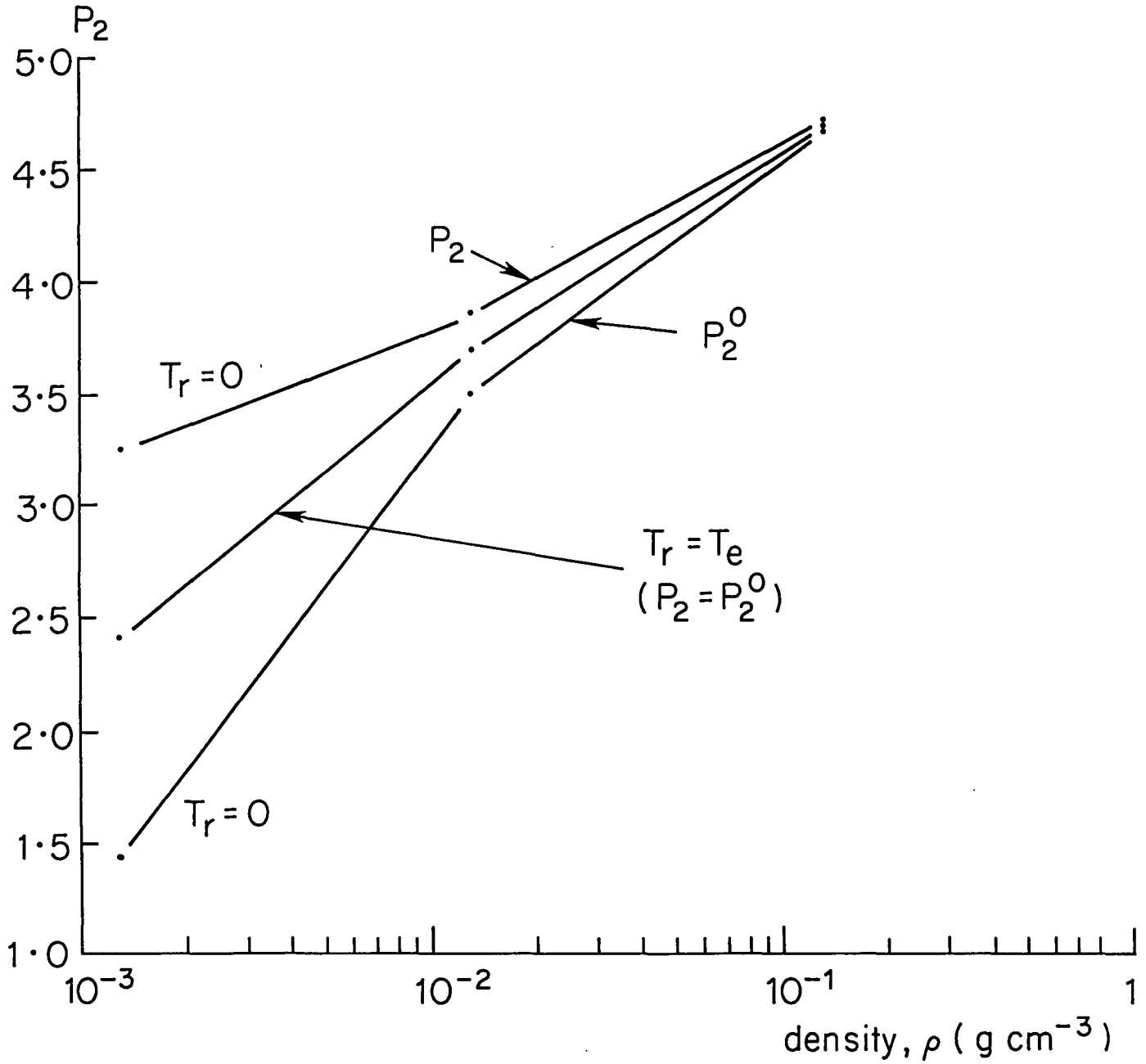
P2
5·0
4·5
4·0
3·5
3·0
2·5
2·0
1·5
1·0
P2
P2^0
Tr = 0
Tr = Te
(P2 = P2^0)
Tr = 0
10^-3
10^-2
10^-1
1
density, ρ (g cm^-3)

Figure 5(a)

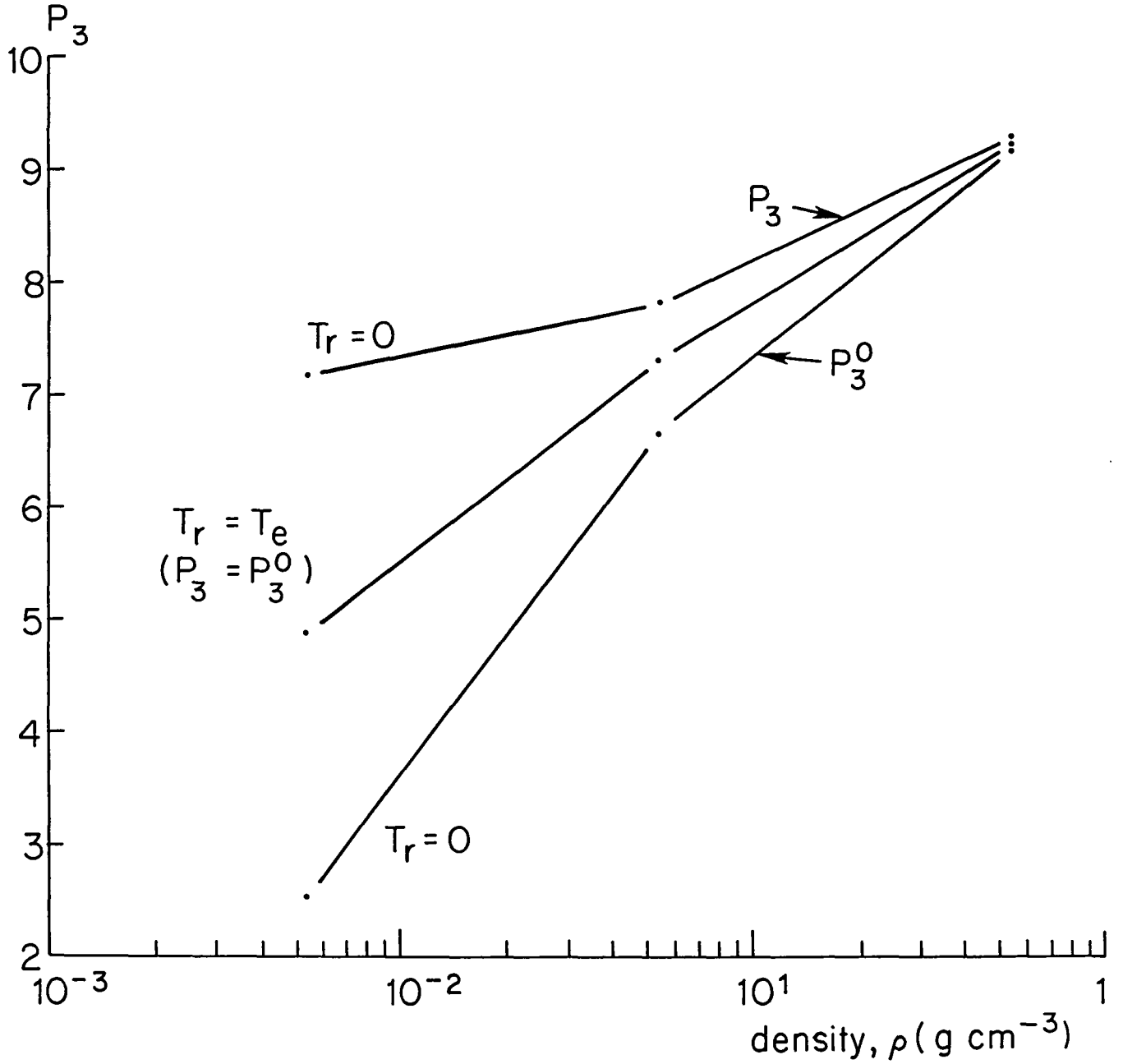
P3
10
9
8
7
6
5
4
3
2
P3
Tr = 0
P3^0
Tr = Te
(P3 = P3^0)
Tr = 0
10^-3
10^-2
10^1
1
density, ρ (g cm^-3)

Figure 5(b)

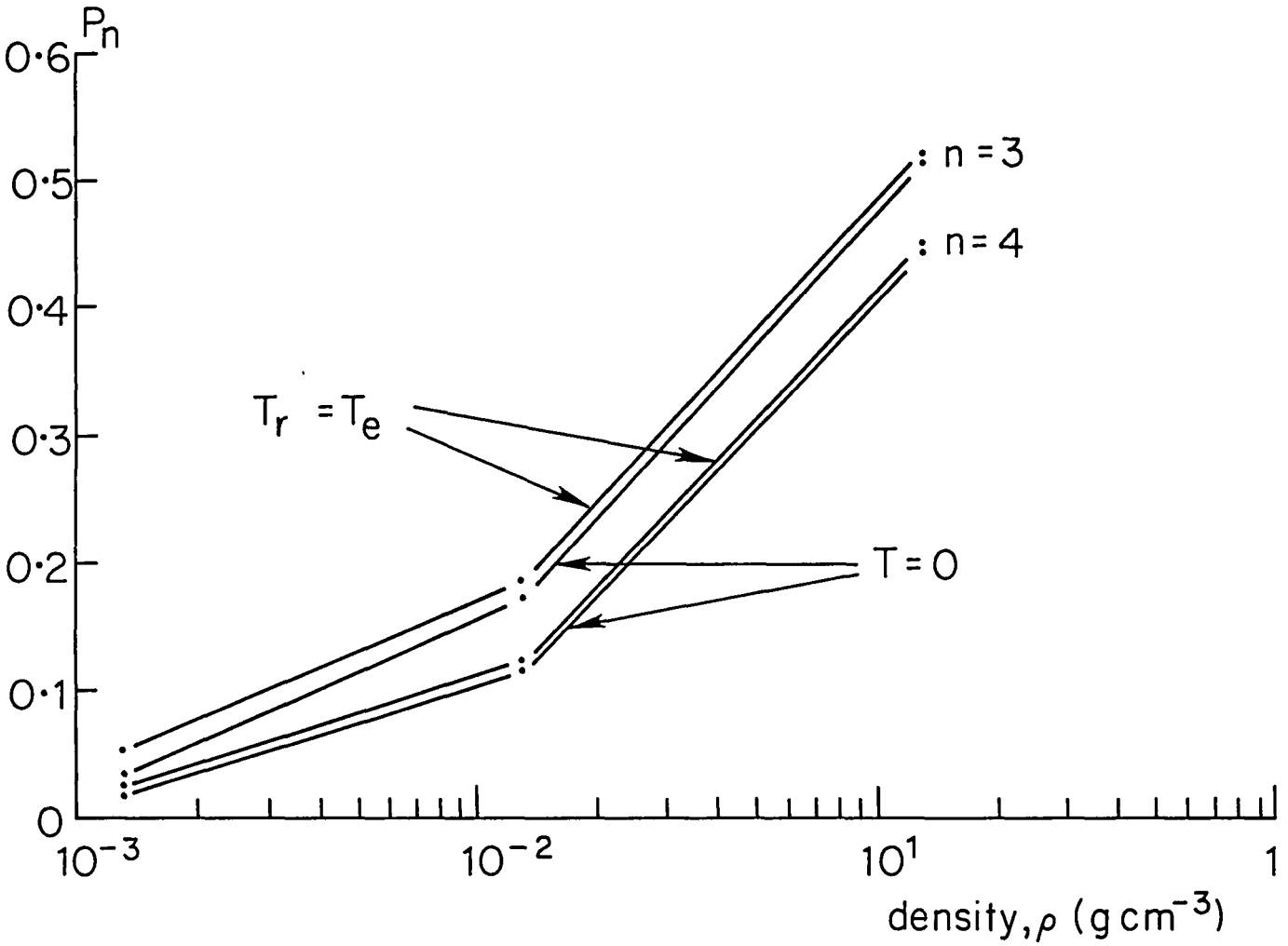

Figure 6(a)

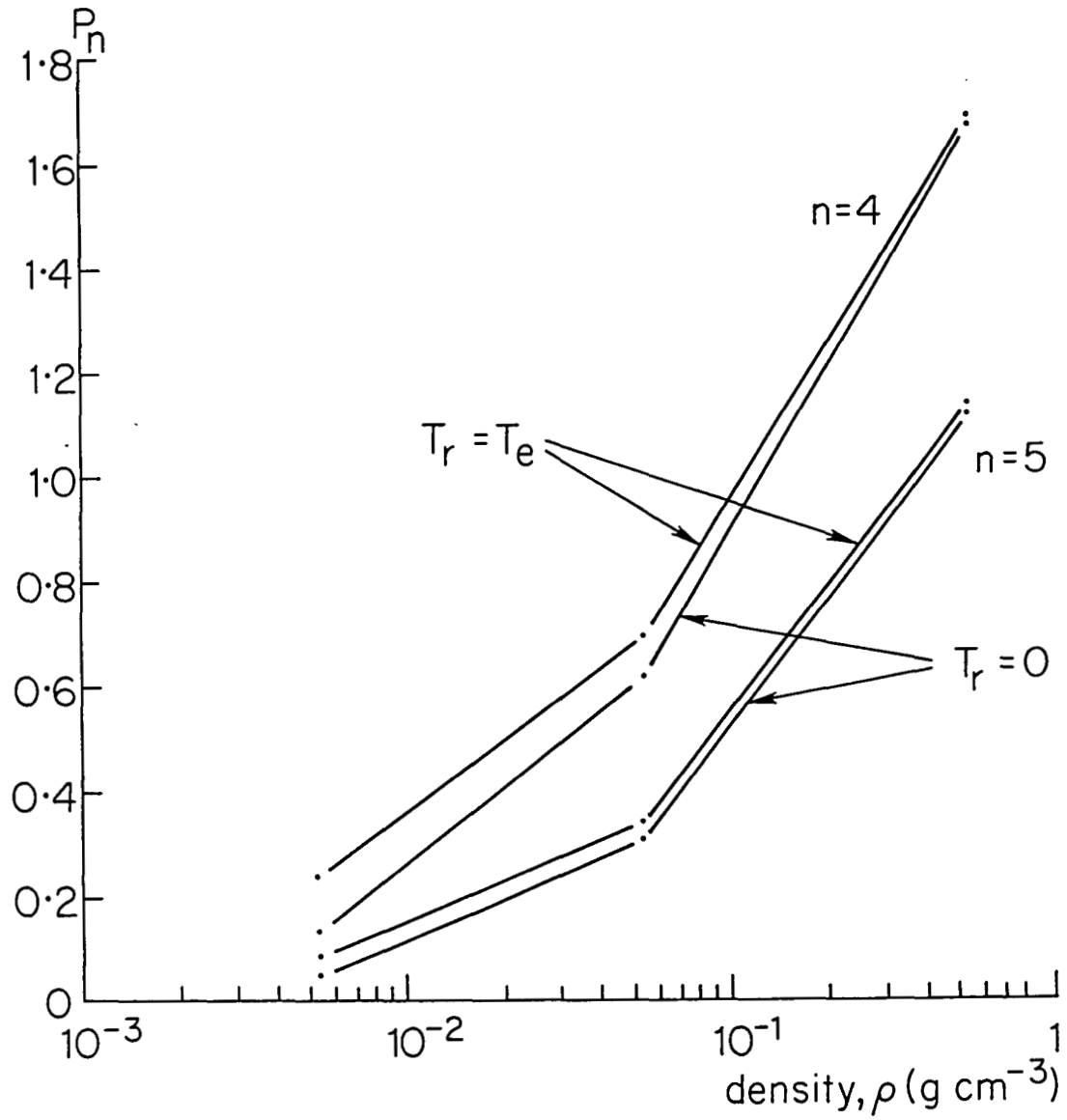
P_n
1·8
1·6
1·4
1·2
1·0
0·8
0·6
0·4
0·2
0
10^{-3}
10^{-2}
10^{-1}
1
density, ρ (g cm^{-3})
n=4
n=5
$T_r = T_e$
$T_r = 0$

Figure 6(b)

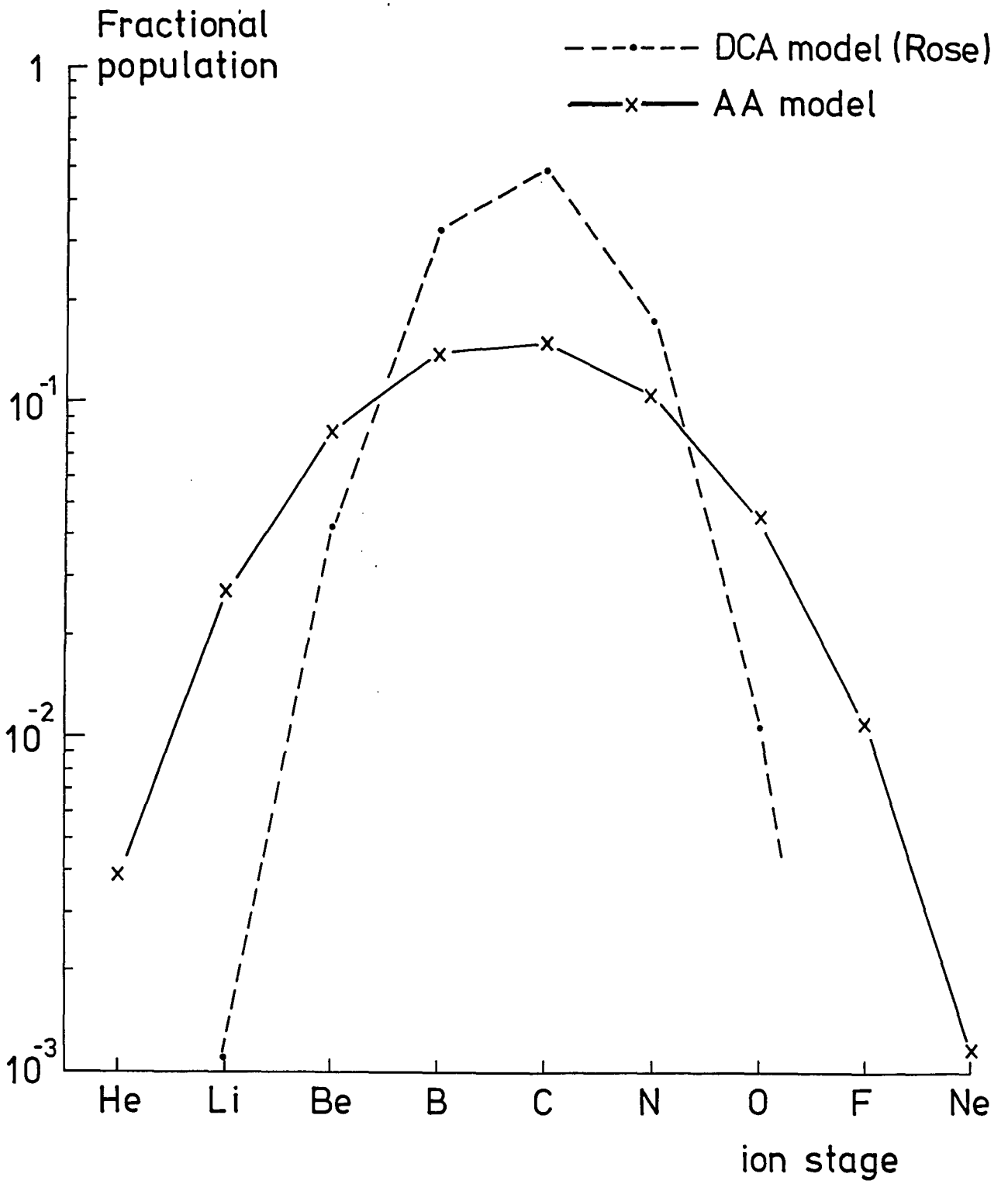
Fractional
population
1
10^{-1}
10^{-2}
10^{-3}
DCA model (Rose)
AA model
He
Li
Be
B
C
N
O
F
Ne
ion stage

Figure 7

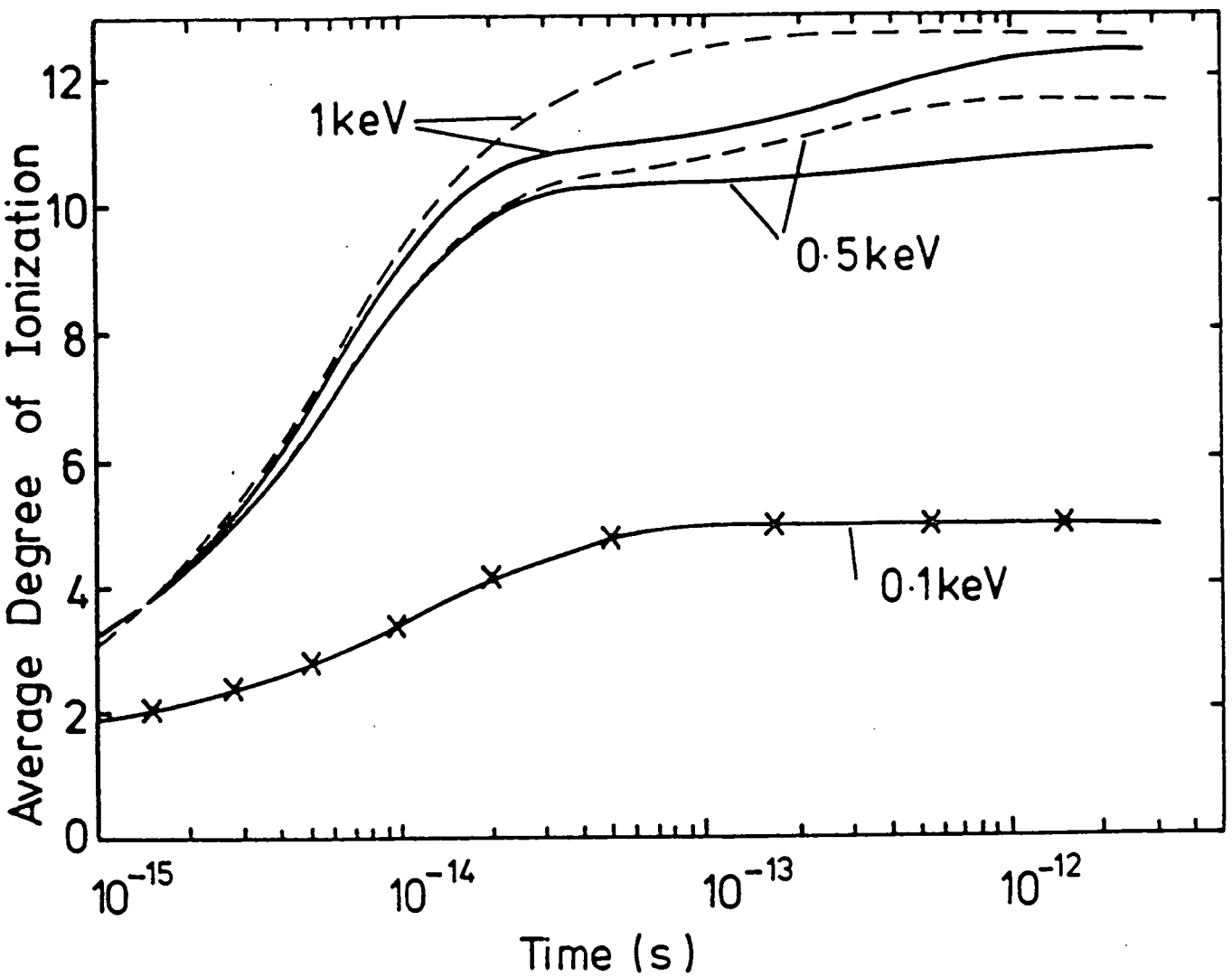
Average Degree of Ionization
0
2
4
6
8
10
12
1keV
0·5keV
0·1keV
10^{-15}
10^{-14}
10^{-13}
10^{-12}
Time (s)

Figure 8(a)

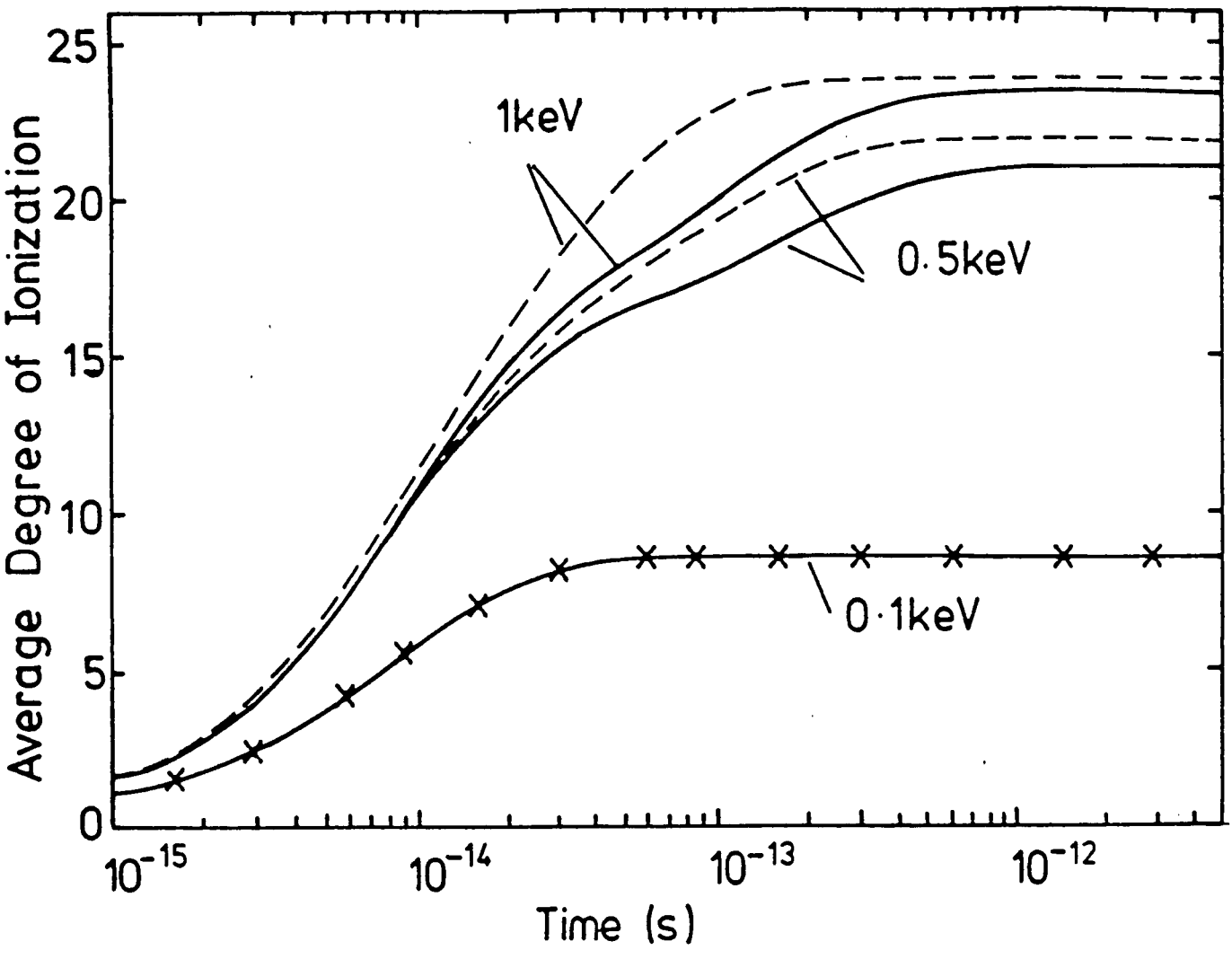
25
20
15
10
5
0
Average Degree of Ionization
1keV
0.5keV
0·1keV
10^{-15}
10^{-14}
10^{-13}
10^{-12}
Time (s)

Figure 8(b)

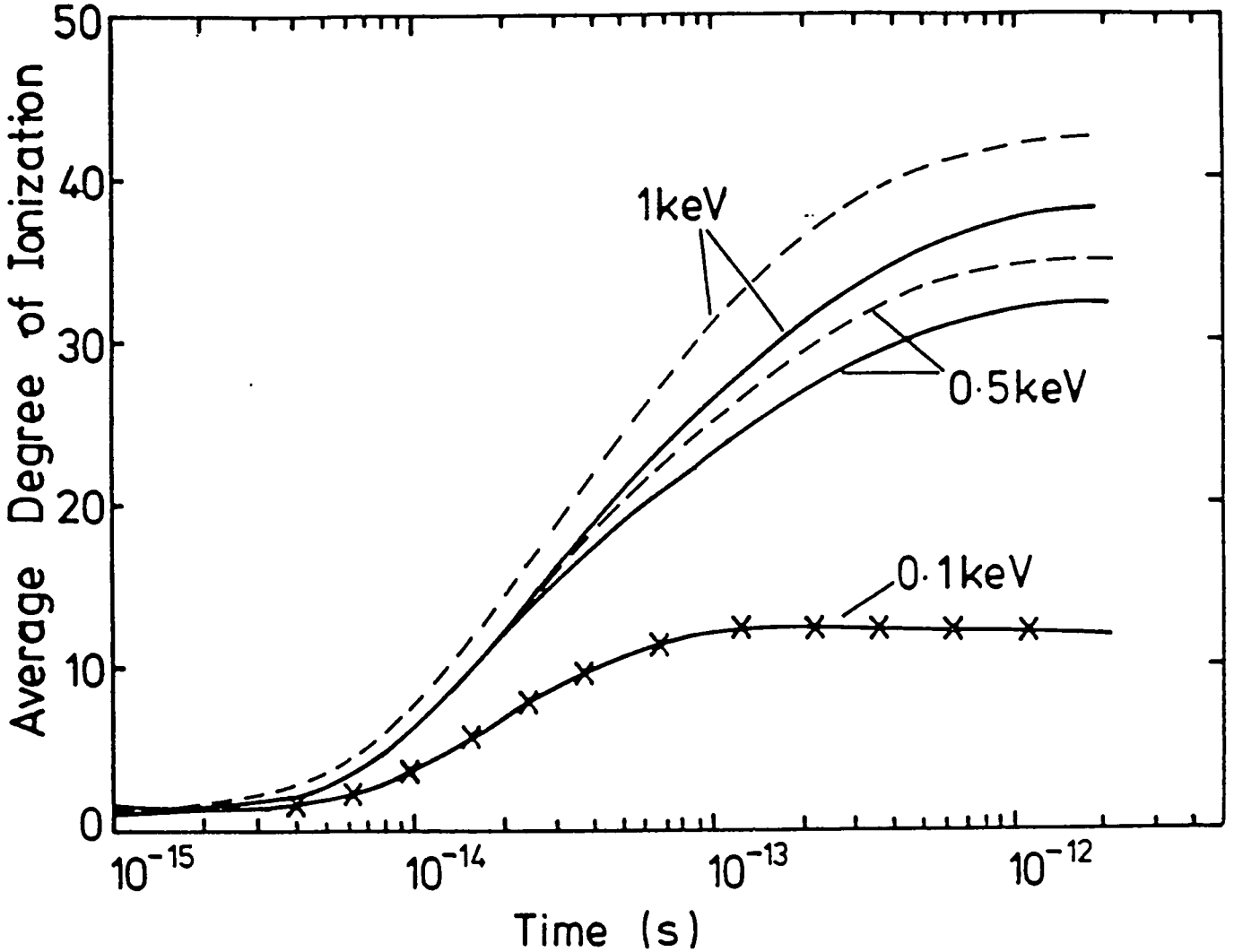
Average Degree of Ionization
50
40
30
20
10
0
1keV
0·5keV
0·1keV
10^{-15}
10^{-14}
10^{-13}
10^{-12}
Time (s)

Figure 8(c)

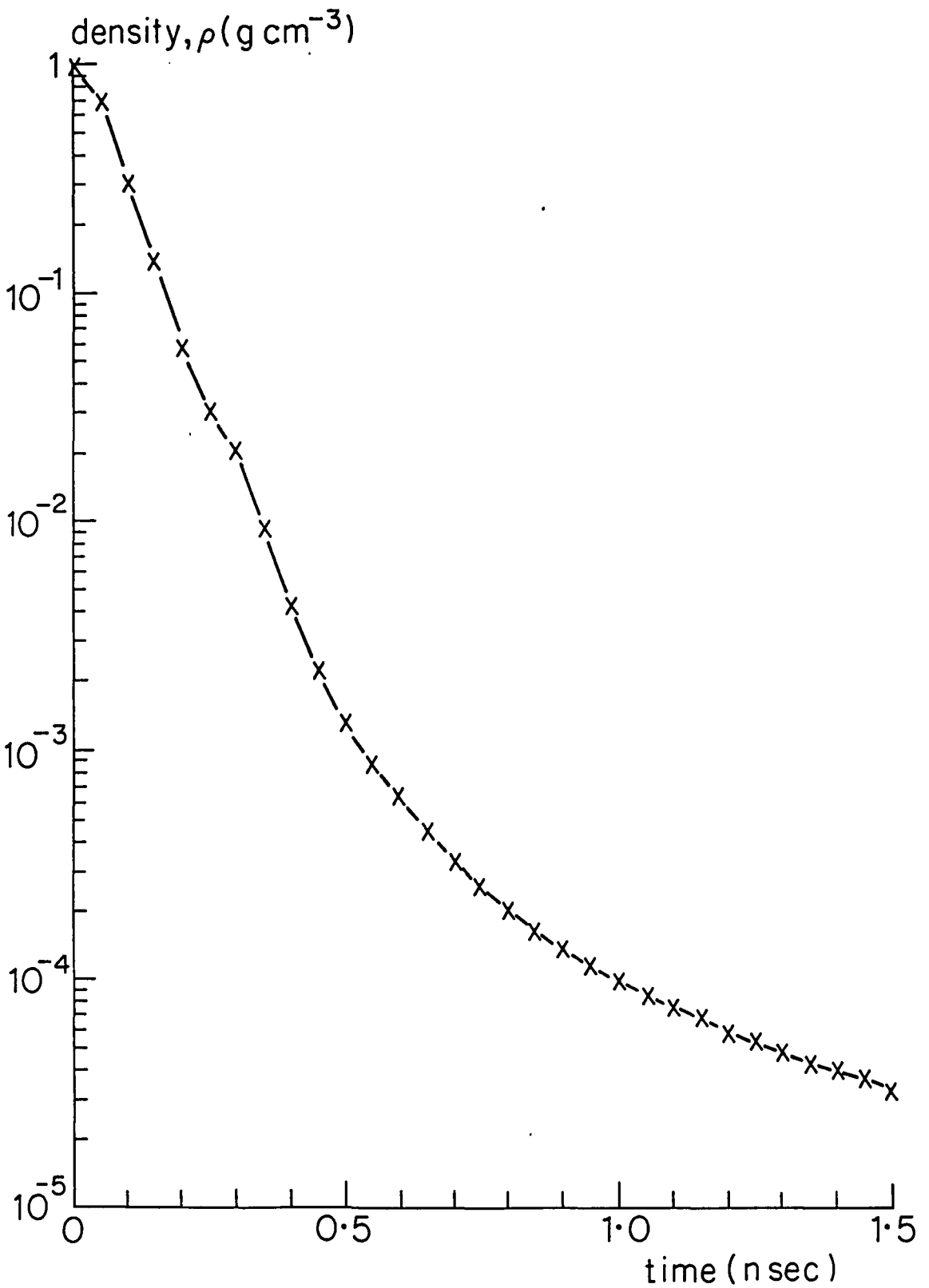

Figure 9(a)

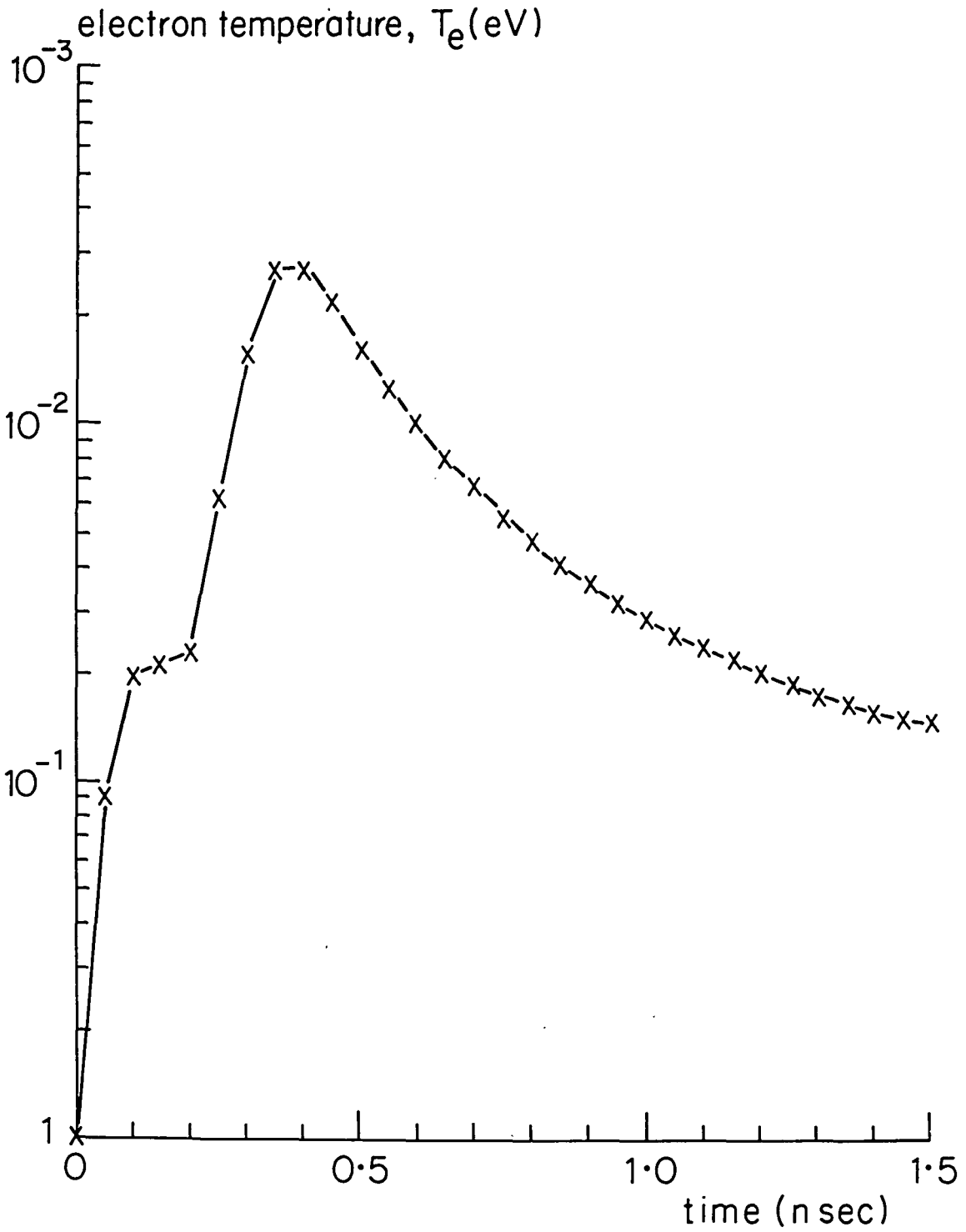

Figure 9(b)

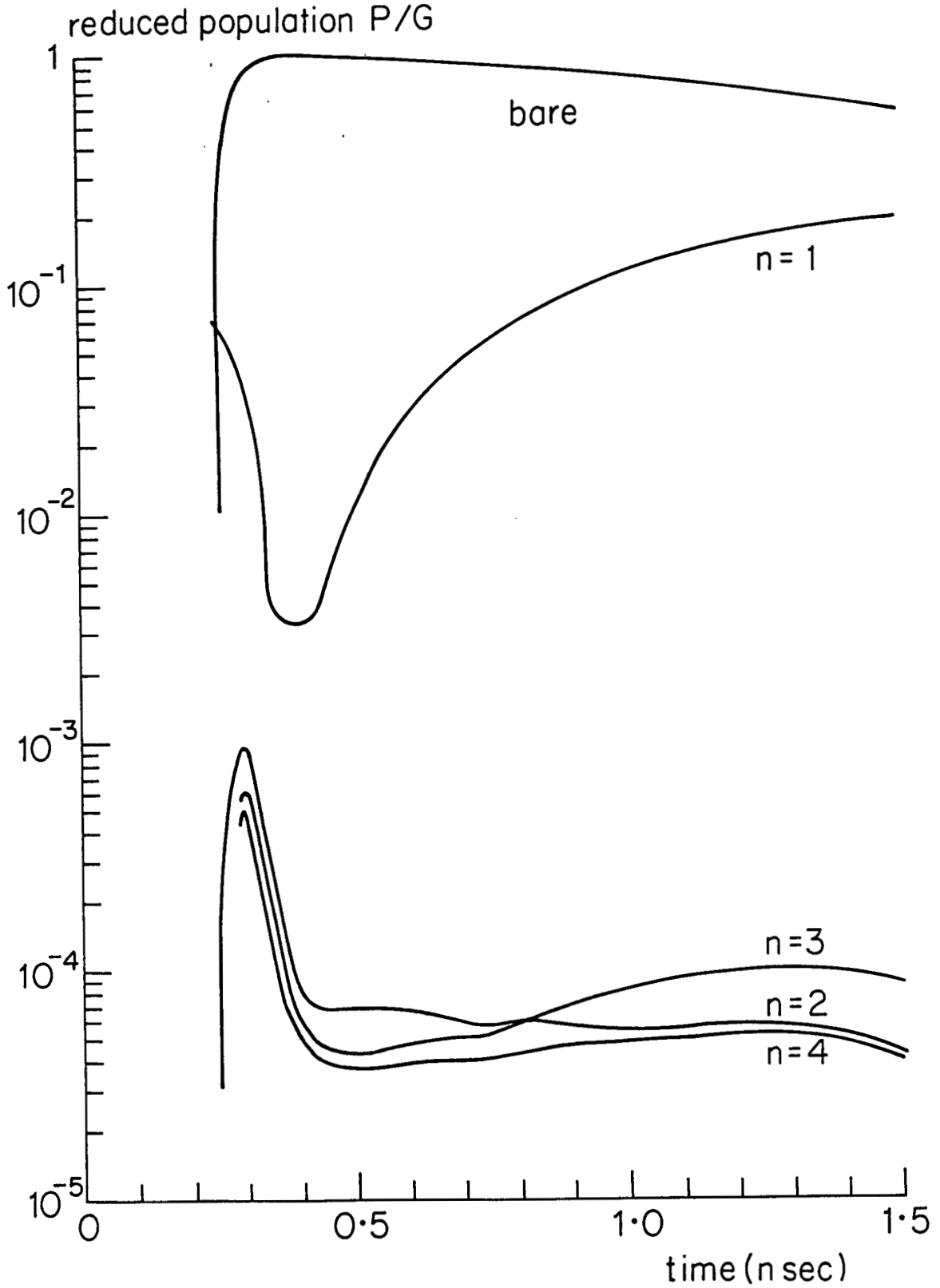
reduced population P/G
1
10^{-1}
10^{-2}
10^{-3}
10^{-4}
10^{-5}
bare
n = 1
n=3
n=2
n=4
0
0·5
1·0
1·5
time (n sec)

Figure 10(a)

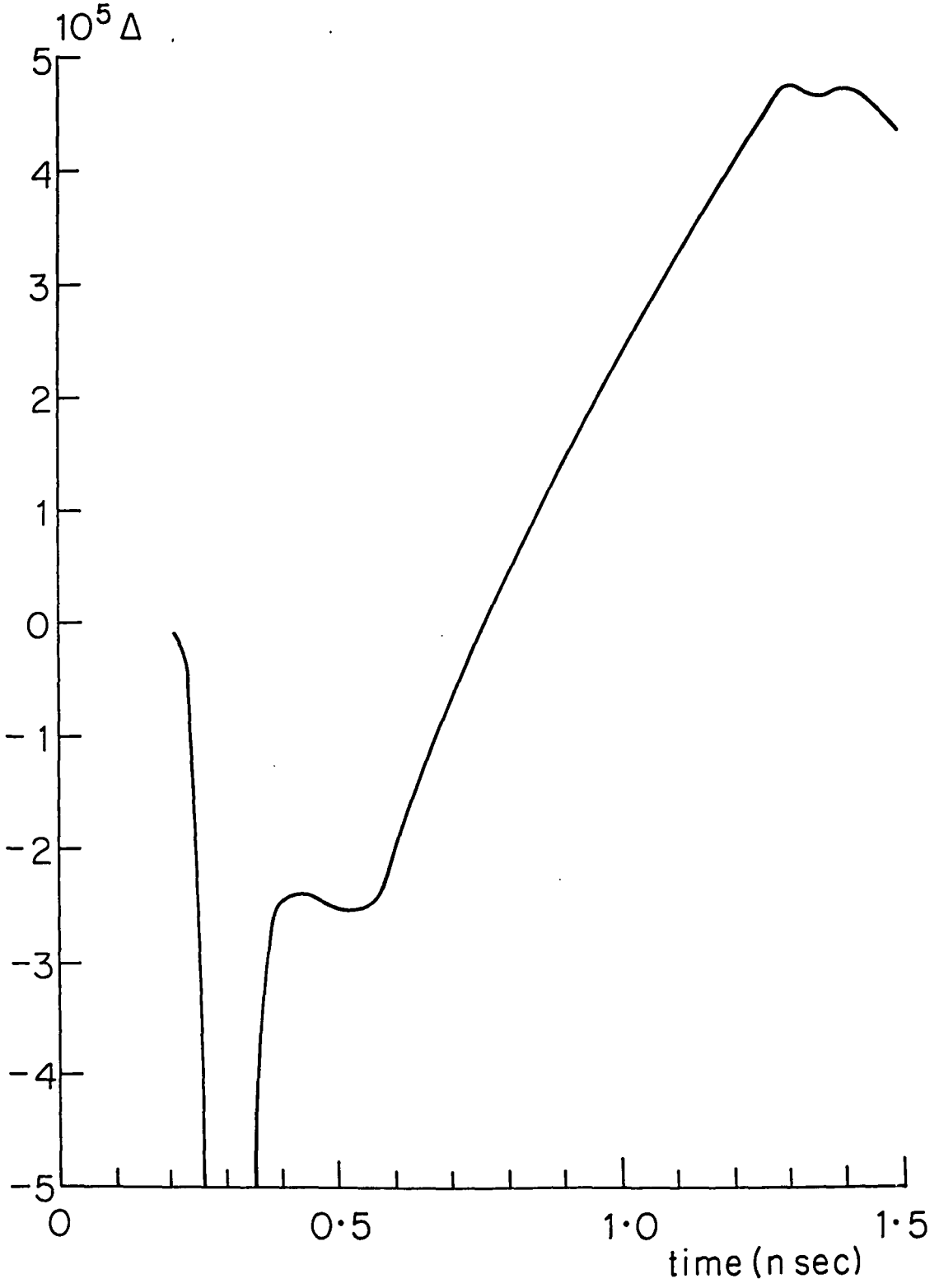

Figure 10(b)